

UARE: A Unified Vision-Language Model for Image Quality Assessment, Restoration, and Enhancement

WeiQi Li¹, Xuanyu Zhang^{1,2}, Bin Chen^{1,2}, Jingfen Xie², Yan Wang², Kexin Zhang²,
Junlin Li², Li Zhang², Jian Zhang^{1†}, Shijie Zhao^{2♦†}
¹School of Electronic and Computer Engineering, Peking University, ²ByteDance Inc.

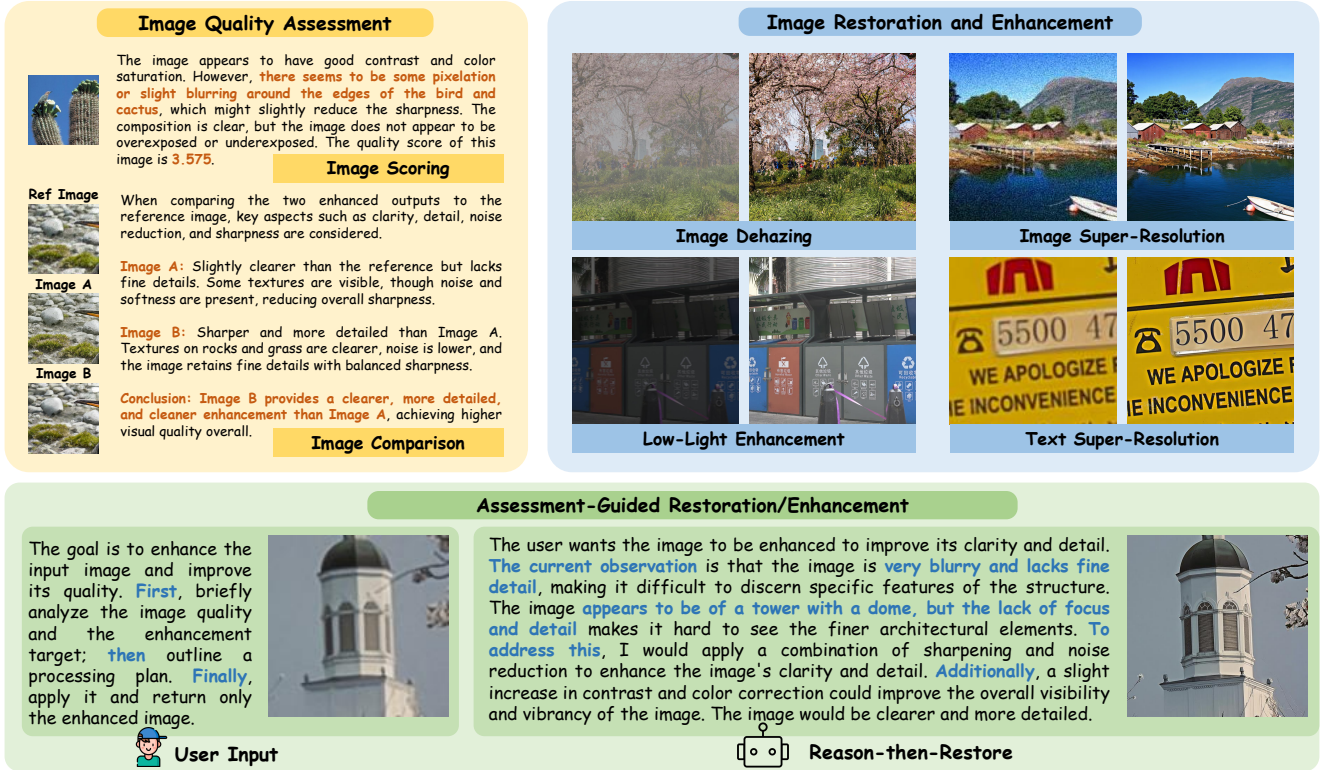


Figure 1. **Showcase of UARE.** It supports image quality assessment (image scoring and comparison), image restoration/enhancement (super-resolution, dehazing, and low-light enhancement, etc.), and assessment-guided restoration and enhancement in **one unified model**.

Abstract

Image quality assessment (IQA) and image restoration are fundamental problems in low-level vision. Although IQA and restoration are closely connected conceptually, most existing work treats them in isolation. Recent advances in unified multimodal understanding-generation models demonstrate promising results and indicate that stronger understanding can improve generative performance. This motivates a single model that unifies IQA and restoration and explicitly studies how IQA can guide restoration, a

setting that remains largely underexplored yet highly valuable. In this paper, we propose **UARE**, to our knowledge the first Unified vision-language model for image quality Assessment, Restoration, and Enhancement. Built on pre-trained unified understanding and generation models, we introduce a two-stage training framework. First, a progressive, easy-to-hard schedule expands from single-type distortions to higher-order mixed degradations, enabling UARE to handle multiple degradations. Second, we perform unified fine-tuning of quality understanding and restoration with interleaved text-image data, aligning IQA signals with restoration objectives. Through multi-task co-training, UARE leverages IQA to boost restoration and enhancement

♦Project Lead. †: Corresponding authors, zhangjian.sz@pku.edu.cn, zhaoshijie.0526@bytedance.com.

performance. Extensive experiments across IQA, restoration, and enhancement tasks demonstrate the effectiveness of UARE. The code and models will be available at <https://github.com/lwq20020127/UARE>.

1. Introduction

Image quality assessment (IQA) [48, 83, 109, 110] and image restoration/enhancement [20, 39, 46, 55, 72, 80, 114] are fundamental, long-standing problems in low-level vision. IQA aims to predict human-perceived quality, either as scalar scores [77, 89, 97, 101] or as natural-language descriptions [43, 99, 100, 113], supporting tasks such as photo selection, camera capture tuning, and large-scale monitoring of streaming and video quality. Image restoration [46, 63, 65, 95, 119] seeks to recover a clean image from a degraded observation, while enhancement [40, 78, 84, 122] improves perceptual quality when no pristine reference is available. Typical applications include real-world photography, perception under adverse weather or low-light conditions, and compression-heavy media delivery.

IQA and restoration are logically closely connected: advances in IQA can guide the design of restoration tools that better match human perceptual preferences, while progress in restoration provides feedback to refine and calibrate IQA. However, most existing work treats them in isolation. On the one hand, IQA methods focus solely on assessment and do not consider compatibility with downstream restoration models. For example, recent multimodal large language model (MLLM)-based IQA methods produce detailed quality descriptions [43, 99, 100, 113] but do not address how restoration methods can leverage such text. On the other hand, most existing restoration methods [42, 79, 95] prioritize producing better results without leveraging IQA context. As a result, the two lines remain largely isolated.

Recently, multimodal understanding and generation have advanced rapidly, with numerous methods jointly optimizing both within a unified architecture [15, 57, 71, 73, 87, 96]. For example, Chameleon [71] treats images as discrete tokens and unifies understanding and generation via next-token prediction. Transfusion [121] integrates diffusion modeling and switches to a diffusion mode at generation time. Bagel [15] employs a mixture-of-transformers (MoT) design, decoupling parameters for understanding and for generation while sharing multimodal self-attention. These approaches achieve strong results and suggest that a stronger understanding improves generation performance in high-level applications. This trend motivates a similar direction in low-level vision: the relationship between IQA and restoration, to some extent, mirrors that between understanding and generation. *Therefore, unifying IQA and restoration in a single model and studying how IQA can guide image restoration and enhancement remains largely*

underexplored and highly valuable.

In this paper, we propose **UARE**, to our knowledge, the first unified vision-language model for image quality assessment, restoration, and enhancement. As shown in Fig. 1, UARE supports image quality assessment tasks such as image scoring and comparison, and restoration tasks such as super-resolution, dehazing, and low-light enhancement. All these tasks are handled by a single model. Notably, UARE also enables assessment-guided restoration in a reason-then-restore style, showing that IQA can benefit restoration. To achieve this, we adopt a two-stage training framework based on a MoT backbone. The first stage employs a progressive easy-to-hard scheme that moves from single-type distortions [42] to higher-order mixed degradations [75, 79], enabling UARE to handle multiple degradations. The second stage performs unified fine-tuning of quality understanding and restoration using interleaved text-image data. This strengthens quality assessment and aligns its signals with restoration objectives. Our empirical study shows that quality assessment boosts restoration performance through multi-task co-training. Extensive experiments across diverse image quality assessment, restoration, and enhancement tasks demonstrate the effectiveness of UARE. In summary, our contributions are:

- We present **UARE**, to our knowledge, the first Unified vision-language model that enables image quality Assessment (image scoring, description, and pairwise comparison) and image Restoration/Enhancement (real-world super-resolution, deblurring, denoising, deraining, dehazing, low-light enhancement, etc.) within a single model.
- We introduce a two-stage training framework: (1) a progressive easy-to-hard training schedule that moves from single-type distortions to high-order mixed degradations; and (2) unified fine-tuning of quality assessment and restoration using interleaved text-image data, aligning assessment signals with restoration objectives.
- We find that image quality assessment boosts restoration through multi-task co-training. Extensive experiments across diverse image quality assessment, restoration, and enhancement tasks demonstrate the effectiveness of UARE.

2. Related Work

2.1. Image Quality Assessment

Traditional studies categorize IQA methods into two paradigms: full-reference and no-reference. Full-reference approaches [68, 83, 109] evaluate the perceptual similarity between a degraded image and its ground-truth counterpart, relying on both classic metrics such as PSNR [83] and learning-based perceptual measures [3, 6, 18, 19, 24, 66] including LPIPS [111]. No-reference IQA methods predict visual quality without access to a clean reference, evolving from handcrafted natural scene statistics [56, 59–62, 67]

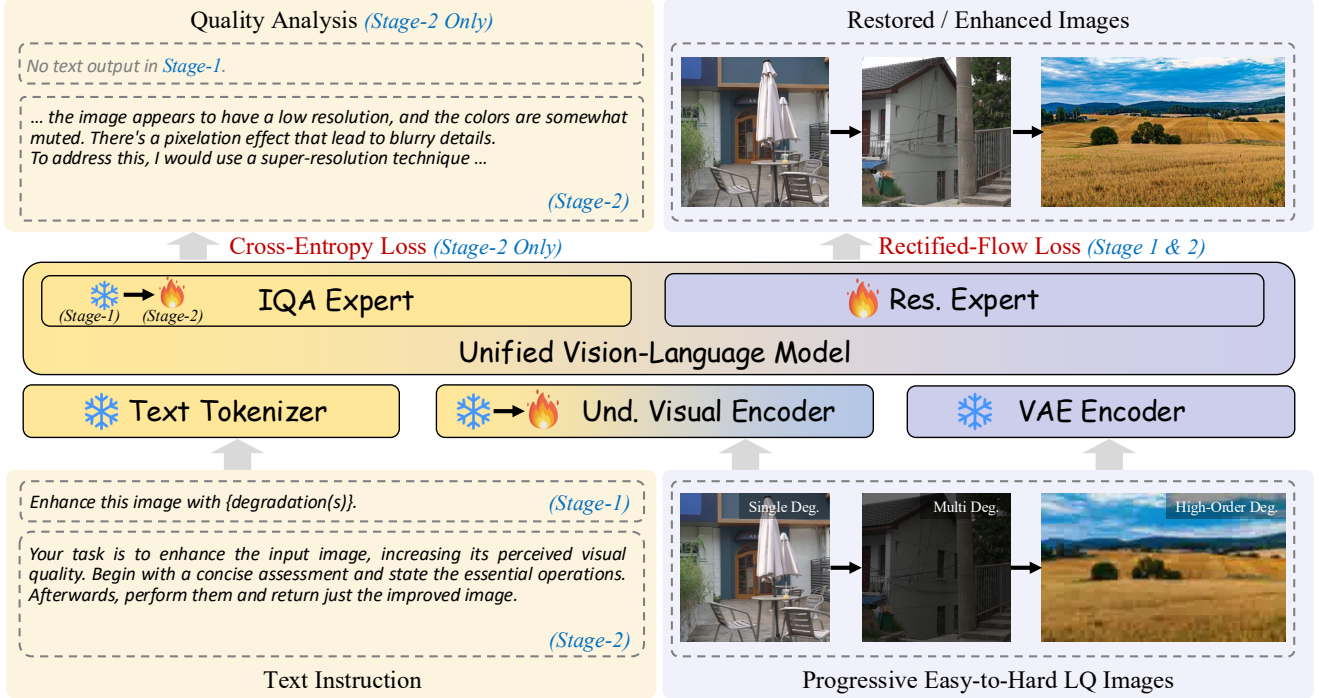


Figure 2. **Illustration of the architecture and two-stage training framework of UARE.** Two transformer experts are used to process IQA and restoration, respectively. Training stages include (1) a progressive, easy-to-hard schedule that moves from single-type to high-order degradations. In this stage, only the restoration expert is trained to make UARE handle multiple degradations. (2) Unified fine-tuning of the entire model to strengthen the IQA ability and align the IQA signals with restoration objectives through interleaved data.

to data-driven neural models that learn quality priors directly from large-scale datasets [33, 34, 52, 64, 69, 70, 77, 120, 123]. With the emergence of multimodal large language models (MLLMs), researchers have begun leveraging their vision-language understanding for image quality evaluation. Score-based frameworks like Q-Align [89] and DeQA-Score [101] generate numerical assessments by exploiting MLLMs’ perception and factual knowledge. Description-driven methods [9, 88, 90, 91, 99, 100, 115–117] emphasize interpretability and richer explanations, typically depending on extensive textual supervision for fine-tuning. Recently, reinforcement learning has been incorporated into IQA tasks [43, 94, 113, 118], enabling models to jointly produce reasoning-based descriptions and quantitative scores, achieving stronger generalization.

2.2. Universal Image Restoration and Enhancement

Image restoration [7, 46, 63] seeks to recover a clean image from a degraded observation, with typical tasks including image super-resolution [49, 82, 93, 103], denoising [29, 58], deblurring [16], and deraining [31], among others. Image enhancement [40, 78, 84, 122] improves perceptual quality when no pristine reference is available, with low-light enhancement as a representative example. Universal image restoration and enhancement aim to handle multiple tasks within a single model, which is challenging because

degradation factors can be distinct and even mutually exclusive [5, 26, 36]. To address this challenge, PromptIR [65] learns input-modulated embeddings that adaptively instruct the network to address different degradations. Diffusion-based methods [51, 95, 119] model degradation distributions using powerful diffusion priors. Pretrained multimodal large models have also been integrated into recent methods [2, 55, 102] to enable high-fidelity, universal image restoration. FoundIR [42] introduces a million-scale dataset covering twenty types of single and mixed degradations and presents a degradation-agnostic generalist model. Our UARE moves beyond existing all-in-one approaches by incorporating IQA capability within a unified model.

2.3. Unified Understanding and Generation

Unified multimodal architectures that jointly support image understanding and generation have emerged as a promising direction. Some methods [12, 71, 81, 87] treat image patches as discrete tokens and generate images with autoregressive next token prediction, as exemplified by Chameleon [71]. Other works [96, 121] integrate diffusion [17] to predict discrete text tokens and to model continuous images. A further line decouples understanding and generation by introducing external diffusion models [11, 30, 47, 73, 76]. Recently, Bagel [15] adopts a mixture-of-transformers (MoT) design and decouples pa-

parameters for understanding and for generation while sharing multimodal self-attention. These methods show promising performance and indicate that improved understanding can enhance generation. In low-level vision, unifying IQA and restoration in a single model and studying how IQA can guide restoration remains largely underexplored and highly valuable. PURE [85] explores joint image degradation estimation and super-resolution within an autoregressive paradigm, but it outputs only simple degradation descriptions and performs only super-resolution. Moreover, PURE has not explored how IQA influences enhancement. Distinctly, our UARE is a more general-purpose unified model for IQA and universal image restoration and demonstrates that IQA can boost restoration.

3. Methodology

3.1. Challenges

Incorporating IQA and restoration into a unified framework presents three significant challenges: *Firstly*, IQA and restoration are distinct tasks with different training objectives. The challenge lies in designing the model such that both tasks can be optimized simultaneously without causing performance degradation due to conflicting goals. *Secondly*, can IQA truly benefit restoration? Specifically, how can the meaningful quality-assessment texts generated by IQA be effectively utilized by restoration? *Thirdly*, within the various sub-tasks of image restoration, degradation types and intensities vary widely. How can the model balance performance across these diverse cases in a unified restoration framework? To address the above challenges, we introduce the network architecture, data construction pipeline, and training framework of UARE as follows.

3.2. Network Architecture

An overview of UARE is illustrated in Fig. 2. UARE is built upon a mixture-of-transformers (MoT) design [15]. Specifically, the network has two full-capacity experts: an IQA expert that receives text tokens from a text tokenizer and image tokens from an understanding visual encoder [74], and a restoration expert that receives VAE [35] latent tokens. Both experts operate on a single interleaved token stream with shared self-attention in every block. The shared context preserves cross-modal alignment, while separate expert parameters reduce gradient interference between IQA and restoration, effectively alleviating task conflict. Illustrations of the three tasks’ data flow are shown below.

IQA: text + image \longrightarrow text. In this task, the input text instruction is firstly tokenized and encoded by the text encoder, and the input image is patched-embedded by the understanding visual encoder. The mixed stream is then processed by the IQA expert to produce an output answer text, while the restoration expert remains inactive.

Image restoration: text + image \longrightarrow image. In text-guided restoration, a short command such as “enhance this image with noise” and a low-quality (LQ) image are fed into UARE together. The IQA expert encodes the command into instruction tokens, inserts these tokens into the shared token stream, and keeps them active in attention. The restoration expert attends to these tokens while processing the VAE latents, uses them to steer the latent updates toward the requested operation, refines the latents, and finally, the decoder produces a high-quality (HQ) image.

Assessment-guided restoration: text + image \longrightarrow text + image. In this task, an instruction such as “analyze the image quality and enhance” and an LQ image are given as input. The IQA expert first generates a compact quality analysis and enhancement recommendations. These analysis tokens remain in the shared stream. The restoration expert conditions on them through shared self-attention when updating the VAE latents. Consequently, the final latents and the decoded HQ image are guided by the analysis, and the model outputs both the analysis text and the restored image.

3.3. Data Construction

Training a unified model requires large, high-quality, and task-diverse data. Notably, to study how IQA can benefit restoration, we construct an interleaved set of quality analysis text–image pairs so that, during training, the restoration expert can condition on outputs from the IQA expert, and both experts are updated in a single pass.

IQA. Our IQA data cover three tasks: image scoring, image degradation description, and image comparison. For image scoring, we utilize KONIQ [28], KADID [48], PIPAL [25], and SPAQ [22]. The input includes an image and a question drawn from a small template pool, and the output is a quality description with a quality score. For image degradation description, the images and corresponding descriptions are obtained from DQ-495K [99]. The images in this dataset include common degradation types such as blur, noise, JPEG artifacts, and low-light, with multiple intensity levels. The descriptions cover both the image content and the specific degradations present in the image. For image comparison, we use DiffQA [10]. Each sample contains a reference image and two super-resolved images produced by different methods. The output is a comparison analysis with quality descriptions for both images, generated using Q-Insight [43] by prompting the model to compare the two results in terms of fidelity and perceptual quality.

Restoration and enhancement. Our restoration and enhancement dataset spans single, multiple, and high-order degradations. Data with single and multiple degradations are obtained from FoundIR [42], which includes blur, noise, JPEG artifacts, haze, rain, and low-light. The multiple degradation data consists of compositions of the individual degradations. For high-order degradations, we fol-

Table 1. **Quantitative comparison of different SR methods** on RealSR, DRealSR, and DIV2K. Throughout this paper, best, second-best, and third-best results are highlighted in **bold red**, underlined blue, *italic green*. \uparrow / \downarrow indicates higher/lower is better.

Test Dataset	Method	PSNR \uparrow	SSIM \uparrow	LPIPS \downarrow	DISTS \downarrow	NIQE \downarrow	LIQE \uparrow	MUSIQ \uparrow	MANIQA \uparrow	TOPIQ \uparrow
RealSR	StableSR [77]	23.73	<i>0.6979</i>	0.2792	<i>0.2023</i>	5.5914	3.0532	61.65	0.3826	0.5201
	DiffBIR [49]	23.20	0.6346	0.3350	0.2162	4.5879	3.5529	65.25	0.4620	0.6033
	SeeSR [93]	<u>24.34</u>	0.7187	<i>0.2754</i>	0.2134	6.4146	3.3938	65.53	<i>0.4856</i>	0.6246
	PASD [98]	24.50	<u>0.7115</u>	0.2716	0.1954	6.0067	2.8541	58.52	0.3831	0.4969
	ResShift [103]	<i>24.17</i>	0.6528	0.4336	0.2812	8.6273	2.6610	53.38	0.3412	0.4210
	SinSR [82]	23.68	0.6649	0.3490	0.2445	6.5101	3.2255	61.03	0.4230	0.5383
	OSDiff [92]	23.07	0.6850	0.2941	0.2109	5.5054	4.0681	<u>68.95</u>	<u>0.4876</u>	<u>0.6441</u>
	S3Diff [106]	23.16	0.6810	<u>0.2748</u>	<u>0.1986</u>	<i>5.3003</i>	<i>4.0080</i>	<i>67.57</i>	0.4677	<i>0.6301</i>
	PURE [85]	21.31	0.5738	0.3859	0.2468	5.6419	3.7881	66.57	0.4829	0.6301
	UARE (Ours)	21.38	0.6464	0.3095	0.2344	<u>5.2981</u>	<u>4.0658</u>	69.67	0.5260	0.6796
DRealSR	StableSR [77]	28.28	0.7981	0.2687	0.2026	7.2816	2.5068	51.62	0.3226	0.4355
	DiffBIR [49]	26.08	0.6578	0.4144	0.2564	4.4856	3.3993	61.81	0.4612	0.6084
	SeeSR [93]	<i>28.14</i>	<u>0.7798</u>	<u>0.2832</u>	0.2241	7.4833	2.7943	55.89	0.3976	0.5436
	PASD [98]	<u>28.18</u>	<i>0.7722</i>	<i>0.2970</i>	<i>0.2108</i>	7.4421	2.6129	51.42	0.3595	0.4587
	ResShift [103]	27.39	0.6907	0.4996	0.3077	9.1788	1.7905	40.58	0.2457	0.3414
	SinSR [82]	26.72	0.6933	0.4031	0.2624	6.8825	2.7781	53.36	0.3677	0.4959
	OSDiff [92]	25.60	0.7403	0.3088	0.2158	<i>6.1544</i>	<u>3.9797</u>	<u>65.24</u>	<u>0.4879</u>	<u>0.6273</u>
	S3Diff [106]	26.18	0.7197	0.3161	<u>0.2099</u>	<u>5.9531</u>	<i>3.9255</i>	<i>63.34</i>	<i>0.4635</i>	<i>0.6181</i>
	PURE [85]	23.04	0.5718	0.4461	0.2674	6.3939	3.7390	60.68	0.4362	0.5888
	UARE (Ours)	21.31	0.5736	0.4071	0.2613	6.4290	4.0445	67.71	0.5121	0.6652
DIV2K	StableSR [77]	19.85	0.4940	0.4796	0.2887	5.7479	1.8466	43.25	0.2181	0.3276
	DiffBIR [49]	18.94	0.4332	0.4009	0.2238	3.6594	3.8573	67.20	0.4574	0.6467
	SeeSR [93]	<i>19.11</i>	<u>0.4580</u>	<i>0.3769</i>	0.2339	4.5817	3.7445	66.31	<i>0.4686</i>	0.6330
	PASD [98]	18.98	0.4562	0.4293	0.2373	4.7846	3.6022	63.46	0.4025	0.5653
	ResShift [103]	<u>19.15</u>	0.4311	0.4900	0.2808	7.4321	2.8862	56.02	0.3534	0.4662
	SinSR [82]	18.58	0.4059	0.4483	0.2455	6.0533	3.4629	64.12	0.4483	0.5997
	OSDiff [92]	18.86	<i>0.4563</i>	<u>0.3579</u>	<i>0.2209</i>	<i>4.1756</i>	3.8877	67.83	0.4422	0.6269
	S3Diff [106]	18.76	0.4490	0.3299	0.1990	4.2026	<u>4.2692</u>	<i>69.31</i>	0.4675	<u>0.6679</u>
	PURE [85]	16.71	0.3661	0.4449	0.2293	4.9545	4.2701	<u>70.06</u>	0.5201	<i>0.6621</i>
	UARE (Ours)	16.59	0.3857	0.4074	<u>0.2138</u>	<u>3.7931</u>	<i>4.2627</i>	70.45	<u>0.5028</u>	0.6864

low the degradation processes used in RealESRGAN [79] and APISR [75], applying degradation sequences to HQ ground-truth images from LSDIR [44] and FoundIR [42]. Across all tasks, HQ images are cropped so that the longer side is 1024 pixels. For high-order degradations, we apply a final downsampling by a factor of 4. For single and multiple degradation tasks, the input instruction is “enhance this image with degradation”. For high-order degradation tasks, the input text is “enhance this mix-degraded image.”

t Building on the LQ-HQ image pairs from the above restoration datasets (with simple instructions), we create interleaved data that incorporates more detailed input and output text descriptions. Specifically, we generate input instructions from a prompt pool following an analyze-then-restore style, such as: “Enhance the input image. Provide a brief analysis of defects and the target appearance, outline the main steps to address them, then apply the enhance-

ments and return the improved image.” The corresponding output text follows a four-step structure, including: (1) user intent, (2) current quality analysis, (3) enhancement plan, and (4) expected result. This structure enables the model to explicitly link quality analysis with restoration actions in a coherent and structured manner.

3.4. Two-Stage Training Framework

As shown in Fig. 2, we adopt a two-stage training framework, using a dynamic mixture of the curated data described above. Further illustrations are given below.

Stage 1: Progressive easy-to-hard restoration training. In this stage, we train only the restoration expert and keep all other components frozen. Using restoration data with simple instructions, UARE first learns to handle diverse degradations. As shown in Fig. 2, the output is the restored image only, without text. Notably, we adopt a progressive

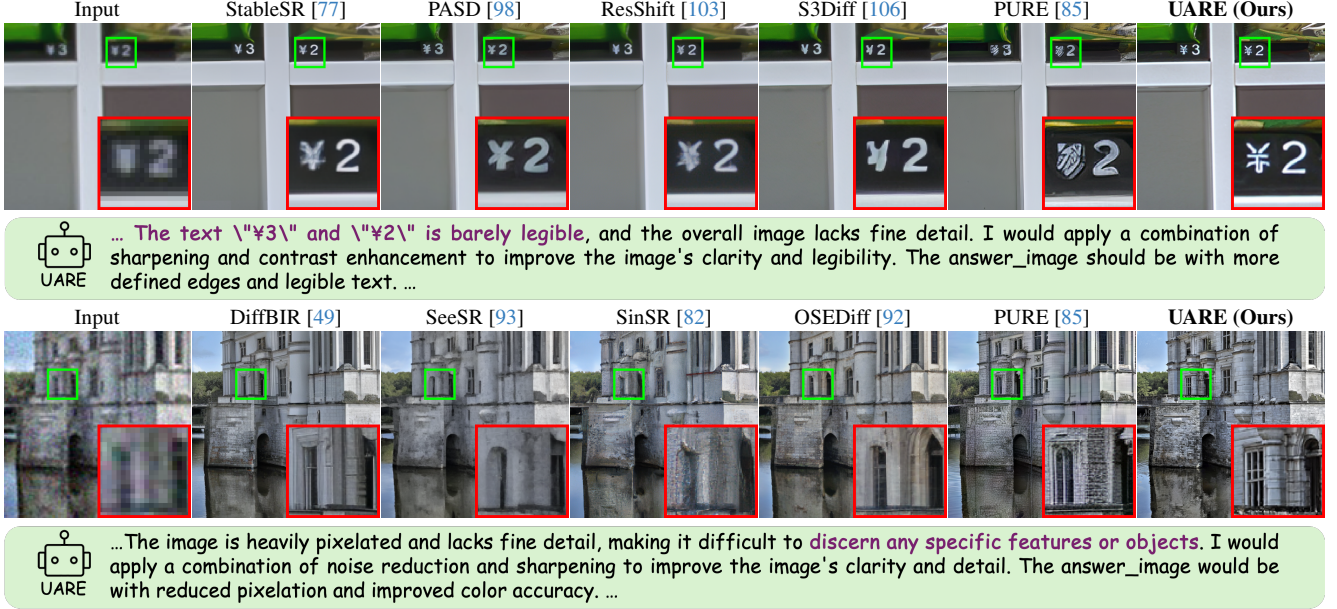


Figure 3. **Visual comparison of super-resolution** on images named “Canon_047” from RealSR (top) and “0000065” from DIV2K-Val (bottom). Our UARE accurately understands both image content and degradations, achieving superior visual quality.

learning strategy: the model is first trained on single degradations, then on multiple degradations, and finally on high-order degradations. This schedule guides the base model from simple to complex cases and steadily translates its generation capacity into strong restoration ability across degradation types and levels. This stage uses 9.6B image tokens for learning single degradations, 19.2B for multiple degradations, and 1.3B for high-order degradations.

Stage 2: Unified fine-tuning of IQA and restoration. After stage 1 stabilizes the core restoration ability, stage 2 jointly fine-tunes IQA and restoration. As shown in Fig. 2, we update all model parameters except those of the VAE and the text tokenizer, using both IQA data and the interleaved text-image data. The corpus for this stage contains 0.4B IQA text tokens and 4.6B image tokens.

3.5. Training Objectives

Both IQA and restoration training samples contain two parts, “condition” and “response”. “Condition” refers to the task prompt, that is, the input text instruction and input image(s). “Response” refers to the corresponding task targets. Denote a sample by $\mathbf{x} = (\mathbf{x}_{\text{con}}, \mathbf{x}_{\text{res}})$, with total sequence length as l , condition length as l_{con} and response length as l_{res} . Let θ be the set of all trainable parameters in UARE.

Autoregression objective. For text prediction in IQA and IQA-guided restoration, where \mathbf{x}_{con} with length l_{con} contains the input instruction and image, and \mathbf{x}_{res} contains only text tokens, UARE is trained by maximum likelihood, as:

$$\mathcal{L}_{AR}(\theta) = -\mathbb{E}_{\mathbf{x} \sim \mathcal{D}_{\text{IQA}}} \left[\sum_{i=l_{\text{con}}}^{l-1} \log P_{\theta}(\mathbf{x}_{i+1} | \mathbf{x}_1, \dots, \mathbf{x}_i) \right], \quad (1)$$

where \mathcal{D}_{IQA} denotes the IQA data. i is the token index start-

ing from l_{con} . The loss is applied only to tokens in \mathbf{x}_{res} .

Rectified flow objective. For image restoration, \mathbf{x}_{con} contains the input instruction and LQ image. For IQA-guided restoration, \mathbf{x}_{con} also includes the generated quality analysis. The response \mathbf{x}_{res} refers to the restored image. UARE is trained with the rectified flow [21, 50, 53] objective, as:

$$\mathcal{L}_{RF}(\theta) = \mathbb{E}_{\mathbf{x} \sim \mathcal{D}_{\text{res}}, \mathbf{z}_0 \sim \mathcal{N}(0, \mathbf{I})} \left[\|v_{\theta}(\mathbf{z}_t, t | \mathbf{x}_{\text{con}}) - (\mathbf{x}_{\text{res}} - \mathbf{z}_0)\|^2 \right], \quad (2)$$

where $\mathbf{z}_t = t\mathbf{x}_{\text{res}} + (1-t)\mathbf{z}_0$, v_{θ} denotes the velocity neural network with parameter θ , \mathcal{D}_{res} denotes the restoration data, and t is the sampled diffusion timestep.

Overall loss. In stage 1, we use only the restoration loss: $\mathcal{L}_{s1} = \mathcal{L}_{RF}$. In stage 2, we use both losses with a trade-off: $\mathcal{L}_{s2} = \mathcal{L}_{RF} + \lambda \mathcal{L}_{AR}$. We set $\lambda = 0.25$ in all experiments.

4. Experiments

4.1. Experimental Setup

Implementation details. We adopt Bagel [15] as our base model, whose understanding visual encoder uses a ViT architecture [14], and whose VAE is from FLUX [37]. The training data, framework, and objective are detailed in Secs. 3.3, 3.4, and 3.5, respectively. To enable classifier-free guidance [27], we randomly drop text, ViT, and clean-VAE tokens with probability 0.1 each. We train UARE for 10K, 20K, and 1.5K steps in stage 1 for single, multiple, and high-order degradations, respectively, and 10K steps for stage 2. The learning rate is fixed at $2e-5$, with a 500-step warmup. In both stages, we use the AdamW [54] optimizer on 64 NVIDIA H20 (96GB) GPUs. The whole training process takes about one week. More details of our training are

Table 2. **Quantitative comparison** on nine multi-degradation subsets of FoundIR. For each method, the first row lists PSNR/LPIPS and the second row lists NIQE/MANIQA. Note that B., N., J., L., and H. denote Blur, Noise, JPEG compression, Low-light, and Haze, respectively.

Method	B.+N.	B.+J.	L.+H.	L.+B.	L.+N.	L.+J.	L.+B.+N.	L.+B.+J.	L.+N.+J.
Restormer [105]	22.70 / 0.3521 6.8794 / 0.1268	22.86 / 0.3397 6.1987 / 0.1567	11.33 / 0.7853 7.3745 / 0.2218	11.22 / 0.5734 7.5792 / 0.1801	8.77 / 0.7081 6.4635 / 0.2190	9.98 / 0.5076 5.145 / 0.2466	9.54 / 0.5680 7.3907 / 0.1621	9.43 / 0.5432 6.6094 / 0.1788	10.43 / 0.3227 5.6162 / 0.2560
PromptIR [65]	22.80 / 0.3460 7.7153 / 0.1354	<u>23.00</u> / 0.3677 7.8357 / 0.1718	16.49 / 0.6541 6.8386 / 0.2391	<u>20.31</u> / 0.4606 8.4172 / 0.1615	11.23 / 0.6908 6.9780 / 0.2286	21.48 / 0.3645 5.4345 / 0.2874	<u>22.31</u> / 0.3918 7.3631 / 0.1339	12.57 / 0.5162 8.2483 / 0.1914	23.09 / 0.2091 5.8646 / 0.2915
DiffIR [95]	22.78 / 0.3318 7.0749 / 0.1315	22.98 / 0.3276 7.0271 / 0.1681	20.03 / 0.2843 <u>3.5989</u> / 0.2751	<u>21.94</u> / 0.3631 6.9691 / 0.1508	14.86 / 0.6158 <u>3.3768</u> / 0.2127	<u>26.21</u> / <u>0.1385</u> <u>3.5363</u> / 0.3428	<u>21.74</u> / 0.3558 6.3189 / 0.1325	<u>21.54</u> / 0.3305 6.4128 / 0.1601	<u>32.14</u> / <u>0.0532</u> <u>4.6687</u> / 0.3000
DiffUIR [119]	<u>26.40</u> / <u>0.1871</u> 5.9532 / <u>0.2660</u>	22.64 / 0.2459 6.2941 / 0.2671	<u>20.50</u> / <u>0.2586</u> <u>3.5501</u> / <u>0.3081</u>	19.28 / <u>0.2934</u> <u>6.4805</u> / <u>0.2470</u>	14.39 / <u>0.4614</u> 4.8987 / 0.2812	20.42 / <u>0.1256</u> 3.9225 / <u>0.3967</u>	19.35 / <u>0.2380</u> <u>5.9545</u> / <u>0.2469</u>	19.52 / <u>0.2950</u> 6.7564 / <u>0.2571</u>	21.68 / 0.0800 5.0353 / <u>0.3358</u>
SUPIR [102]	21.58 / 0.2533 <u>4.1727</u> / <u>0.3330</u>	21.36 / 0.3335 <u>4.9403</u> / <u>0.3053</u>	10.34 / 0.6731 4.9167 / 0.2753	10.75 / 0.5520 7.8850 / 0.1815	8.39 / 0.7636 7.5038 / 0.1973	8.22 / 0.4148 4.3194 / 0.3418	9.47 / 0.5456 7.3296 / 0.1594	9.14 / 0.5174 7.8990 / 0.2078	8.72 / 0.2817 5.0521 / 0.3065
InstructIR [13]	21.52 / 0.2455 <u>5.8400</u> / 0.1768	21.40 / <u>0.2067</u> <u>6.0394</u> / 0.2511	13.71 / 0.5406 4.0786 / 0.2880	17.59 / 0.3900 6.7789 / 0.1558	<u>16.80</u> / 0.5926 <u>3.0146</u> / <u>0.2846</u>	18.69 / 0.2008 <u>3.4827</u> / 0.3616	12.61 / 0.4020 6.1334 / 0.1571	17.55 / 0.3447 <u>6.2047</u> / 0.1709	19.17 / 0.0929 <u>4.0862</u> / 0.3191
AutoDIR [32]	21.74 / 0.3092 6.9000 / 0.1541	22.14 / 0.3098 7.0662 / 0.1847	14.77 / 0.6757 6.9955 / 0.1964	19.58 / 0.4300 7.6655 / 0.1691	<u>17.73</u> / 0.5235 6.6220 / 0.2198	16.48 / 0.4028 5.8992 / 0.2803	18.37 / 0.3971 7.0586 / 0.1662	17.19 / 0.3706 7.2479 / 0.2006	18.89 / 0.2056 5.6556 / 0.2766
FoundIR [42]	<u>23.81</u> / <u>0.2387</u> 6.1397 / 0.2282	<u>30.60</u> / <u>0.1551</u> 6.4299 / <u>0.2851</u>	<u>23.86</u> / <u>0.2774</u> 4.1639 / <u>0.3033</u>	<u>25.13</u> / <u>0.2282</u> <u>6.2341</u> / <u>0.2398</u>	<u>16.47</u> / <u>0.4054</u> 5.5928 / <u>0.3285</u>	<u>30.32</u> / <u>0.0960</u> 3.8810 / <u>0.4067</u>	<u>23.60</u> / <u>0.2231</u> <u>5.7256</u> / <u>0.2452</u>	<u>22.79</u> / <u>0.2183</u> <u>6.3009</u> / <u>0.2629</u>	<u>34.27</u> / <u>0.0559</u> 4.9494 / <u>0.3360</u>
UARE (Ours)	<u>25.16</u> / <u>0.1573</u> <u>4.8956</u> / <u>0.2970</u>	<u>29.55</u> / <u>0.0891</u> <u>4.9061</u> / <u>0.3446</u>	<u>20.10</u> / <u>0.2491</u> <u>3.2736</u> / <u>0.3765</u>	20.08 / <u>0.1878</u> <u>4.5594</u> / <u>0.3245</u>	15.08 / <u>0.3875</u> <u>4.5500</u> / <u>0.3738</u>	<u>23.01</u> / 0.1540 <u>3.2550</u> / <u>0.3999</u>	20.20 / <u>0.1777</u> <u>4.6937</u> / <u>0.3169</u>	<u>24.09</u> / <u>0.1225</u> <u>5.0266</u> / <u>0.3379</u>	<u>29.30</u> / <u>0.0659</u> <u>4.5995</u> / <u>0.3353</u>

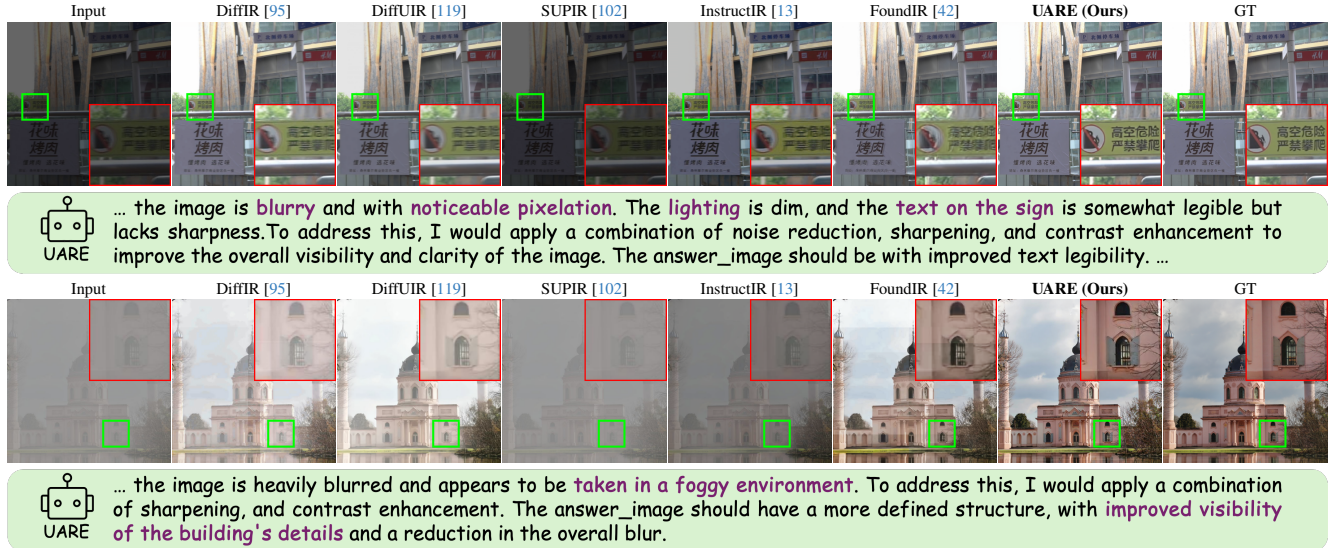


Figure 4. **Visual comparison** on images named “1426” with low-light, blur, and noise (top), and “0525” with haze (bottom) from FoundIR.

provided in the [supplementary materials](#).

4.2. Super Resolution

Settings. Following [92, 93, 106], we evaluate UARE and compare it with prior methods on center-cropped RealSR [4], DRealSR [86], and DIV2K [1] with 512×512 resolution, performing $4\times$ SR. We compare UARE against eight diffusion-based methods: StableSR [77], DiffBIR [49], SeeSR [93], PASD [98], ResShift [103], SinSR [82], OSediff [92], S3Diff [106], and the autoregressive method PURE [85]. We adopt both full- and no-reference metrics for evaluation. For reference-based fidelity, we use PSNR and SSIM [83], calculated on the Y channel in YCbCr space. For reference-based perceptual quality, we apply LPIPS and DISTS. We also utilize

NIQE [110], LIQE [112], MUSIQ [34], MANIQA [97], and TOPIQ [8].

Results. Tab. 1 presents that our UARE achieves strong results across multiple metrics. Firstly, it ranks first in MUSIQ and TOPIQ across all datasets, and top-3 in MANIQA and LIQE. Secondly, it attains PSNR comparable to PURE while achieving better SSIM, LPIPS, and DISTS. Qualitative results are shown in Fig. 3. UARE accompanies restoration with fine-grained, language-aligned quality analysis, correctly diagnosing issues (e.g., “barely legible text,” “heavy pixelation”) and suggesting appropriate enhancements. Moreover, UARE restores clearer text and well-formed window/brick patterns with markedly fewer artifacts. More visual results and a user study are provided in the [supplementary materials](#).

Table 3. **PLCC / SRCC comparison** on the image quality assessment task between our UARE and other competitive methods.

Methods	SPAQ	KADID	LiveW	AGIQA	CSIQ
NIQE [60]	0.679	0.468	0.493	0.560	0.718
(SPL 2012)	/0.664	/0.405	/0.449	/0.533	/0.628
BRISQUE [59]	0.490	0.429	0.361	0.541	0.740
(TIP 2012)	/0.406	/0.356	/0.313	/0.497	/0.556
MUSIQ [34]	0.868	0.575	0.789	0.722	0.771
(ICCV 2021)	/0.863	/0.556	/0.830	/0.630	/0.710
CLIP-IQA+ [77]	0.866	0.653	0.832	0.736	0.772
(AAAI 2023)	/0.864	/0.654	/0.805	/0.685	/0.719
ManIQA [97]	0.768	0.499	0.849	0.723	0.623
(CVPR 2022)	/0.758	/0.465	/0.832	/0.636	/0.627
Q-Align [89]	0.886	0.674	0.853	0.772	0.671
(ICML 2024)	/0.887	/0.684	/0.860	/0.735	/0.737
DeQA [101]	0.895	0.694	0.892	0.809	0.787
(CVPR 2025)	/0.896	/0.687	/0.879	/0.729	/0.744
Q-Insight [43]	0.913	0.757	0.867	0.805	0.768
(NeurIPS 2025)	/0.907	/0.765	/0.830	/0.757	/0.740
UARE	0.902	0.878	0.855	0.752	0.930
(Ours)	0.898	0.873	/0.814	/0.667	0.915

4.3. Mix-Degraded Image Restoration

Settings. We evaluate UARE and compare it with other methods on the center-cropped FoundIR test set [42] with 1024×1024 resolution. We compare UARE against eight state-of-the-art restoration methods: Restormer [105], PromptIR [65], DiffIR [95], DiffUIR [119], SUPIR [102], InstructIR [13], AutoDIR [32], and FoundIR [42]. We adopt PSNR, LPIPS, NIQE, and MANIQA as evaluation metrics.

Results. Tab. 2 shows that our UARE achieves top-3 performance on nearly all metrics across the mixed-degradation subsets of FoundIR. Fig. 4 shows that UARE precisely identifies degradation types and scene content in LQ inputs, removes blur, low-light, noise, and haze, and reconstructs vivid, realistic details in challenging regions (e.g., fine facade structures and small text). Results on single-degradation subsets are given in [supplementary materials](#).

4.4. Image Quality Assessment

We compare UARE with handcrafted methods NIQE [60] and BRISQUE [59], non-LLM approaches MUSIQ [34], CLIP-IQA+ [77], MANIQA [97], and LLM-based methods Q-Align [89], DeQA-Score [101], and Q-Insight [43]. Following Q-Insight [43], we evaluate on SPAQ [22], KADID [48], LIVEW [23], AGIQA [41], and CSIQ [38]. PLCC and SRCC are adopted for image score regression. As shown in Tab. 3, UARE significantly surpasses the current state-of-the-art IQA method Q-Insight on KADID and CSIQ, while achieving comparable performance on the remaining benchmarks. It demonstrates that our method not only achieves superior reconstruction performance but also possesses strong visual quality understanding capability.

Table 4. **Ablation study** of the two-stage training framework.

Methods	PSNR↑	LPIPS↓	LIQE↑	MUSIQ↑	MANIQA↑
Pretrained Bagel	21.00	0.5906	1.0990	29.66	0.1792
+ single deg.	22.26	0.4205	1.0080	28.10	0.2033
+ multi deg.	21.17	0.3989	1.0235	30.96	0.2152
+ high-order deg.	22.74	0.2603	3.5686	60.21	0.4082
All-in-one stage	23.65	0.2662	2.8750	57.50	0.3760
UARE (Ours)	21.38	0.3095	4.0658	69.67	0.5260

Table 5. **Ablation study** of the IQA guidance in restoration.

Methods	PSNR↑	LPIPS↓	LIQE↑	MUSIQ↑	MANIQA↑
Simple prompt	21.79	0.2772	3.6308	66.52	0.4668
Q-Insight prompt	21.26	0.3175	4.0498	64.43	0.4817
UARE (Ours)	21.38	0.3095	4.0658	69.67	0.5260

4.5. Ablation Study

Effect of two-stage training. In Tab. 4, we show the results of pretrained Bagel and three variants after each progressive step in stage 1 on the RealSR dataset. We also train an “all-in-one stage” variant by mixing all data in a single-stage training. Our progressive training framework balances fidelity and perceptual quality, achieving the best overall performance. Besides, comparing the “+ high-order deg.” variant with our final UARE confirms that introducing IQA data to jointly fine-tune the IQA and restoration experts yields a significant gain in perceptual quality.

Effect of the IQA guidance in restoration. In Tab. 5, we study how different text prompts used at inference affect UARE’s restoration performance on RealSR. Specifically, the “single prompt” setting uses the instruction “enhance the mix-degraded image.” The “Q-Insight prompt” first asks the Q-Insight model to produce a degradation analysis and enhancement suggestions, then feeds those suggestions as textual instructions together with the low-quality image into UARE. Our UARE follows an analysis-then-restore paradigm: it outputs a quality analysis first, and then the enhanced image. UARE achieves the best perceptual metrics while maintaining comparable fidelity. Compared with the single-prompt setting, UARE parses and exploits richer IQA textual information. Compared with the Q-Insight-prompt setting, UARE aligns its own IQA and restoration capabilities more effectively, thereby turning IQA insights into concrete gains in restoration.

5. Conclusion

In this paper, we propose UARE, a novel unified vision-language model for image quality assessment, restoration, and enhancement. We introduce a two-stage training framework. The first stage enables UARE to handle multiple degradations in a progressive way, while the second stage aligns IQA signals with restoration objectives. We find that IQA can boost the restoration performance of UARE through multi-task co-training. Extensive experiments across diverse tasks demonstrate the effectiveness of

UARE. Looking ahead, UARE can extend its capabilities to a wide range of tasks, such as video quality understanding and restoration. As a unified model, UARE has the potential to revolutionize IQA and restoration/enhancement, providing a unified solution that can transform how image quality is evaluated, improved, and applied across various fields.

Supplementary Material

Our main paper presents the core ideas, architecture, and experimental results of UARE, a unified vision–language model for image quality assessment, restoration, and enhancement. In this [supplementary material](#), we provide additional information. Sec. A gives implementation details, including representative data examples in Sec. A.1 and training configurations in Sec. A.2. Sec. B reports more comparison results, with real-world super resolution in Sec. B.1, image restoration/enhancement in Sec. B.2, and a user study in Sec. B.3. Finally, Sec. C offers further discussion of UARE and a detailed analysis of its limitations.

A. Implementation Details

A.1. Data Examples

We have detailed the data construction process in our main paper. Here, we provide data examples for training UARE in Fig. A.1 and Fig. A.2 for IQA and restoration/enhancement, respectively. For IQA, our data include diverse instruction formats such as free-form quality description, scalar quality scoring, and reference-based pairwise comparison. For restoration and enhancement, we construct instructions for single, multiple, and high-order degradations, as well as interleaved text–image data where the model must first analyze the degradation and user intent and then plan the enhancement steps. These examples span

a wide range of scenes (indoor/outdoor, day/night, natural and urban) and degradation types (blur, low light, noise, haze, and complex mixed artifacts), highlighting the richness and compositionality of our training corpus.

A.2. Training Details

Table A.1 summarizes the full training recipe of UARE. For all stages, we use a constant learning rate of 2×10^{-5} , zero weight decay, gradient-norm clipping of 1.0, and AdamW ($\beta_1 = 0.9$, $\beta_2 = 0.95$, $\epsilon = 1.0 \times 10^{-15}$) with EMA ratios of 0.990, 0.995, 0.995, and 0.995 for the single-degradation, multi-degradation, high-order degradation, and unified fine-tuning stages, respectively. The three stage-1 curricula are trained for 10K, 20K, and 1.5K steps with 250 warm-up steps, while the unified stage is trained for 10K steps with a 500-step warm-up. In the unified stage, we jointly optimize the IQA cross-entropy loss and the restoration MSE loss with a weight ratio of 0.25 : 1. Restoration images are randomly resized such that the minimum short side and maximum long side fall in (512, 1024), and IQA images are resized to (378, 980). We apply a diffusion timestep shift of 4.0 for all diffusion-based restoration branches. The bottom part of Table A.1 lists the data sampling ratios: stage-1 curricula only sample their corresponding degradation type (single, multi, or high-order), whereas the unified stage mixes IQA, single-, multi-, and high-order degradation data and interleaved IQA–restoration pairs, forming a balanced curriculum for learning unified quality assessment and restoration.

B. More Comparison Results

B.1. Real-World Super Resolution

More quantitative results. We further report more quantitative results in Tab. B.1 on RealSR [4], DRealSR [86]

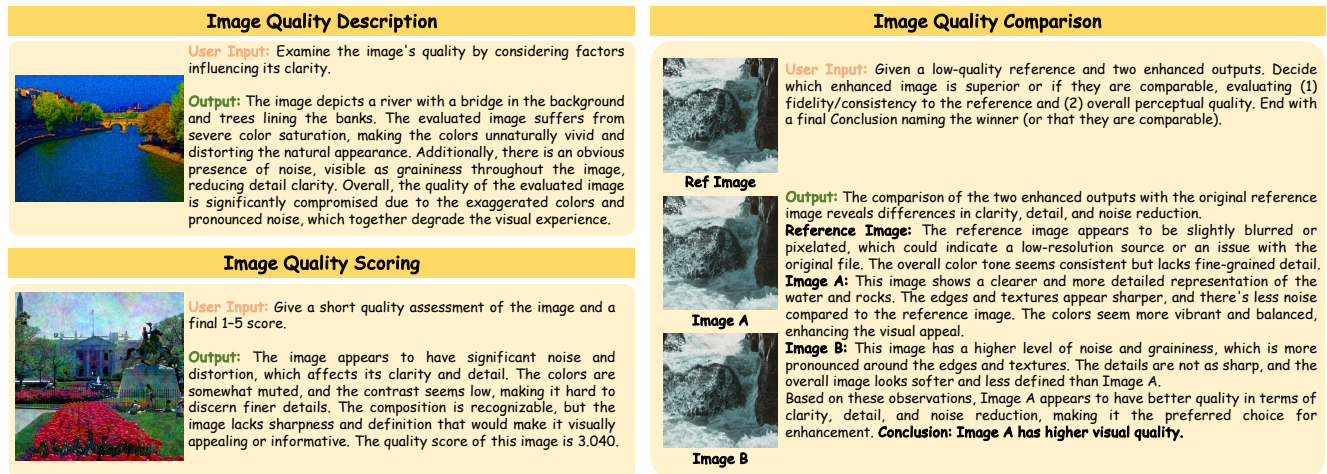


Figure A.1. Data examples for IQA training in UARE, including quality description, image quality scoring, and image comparison.

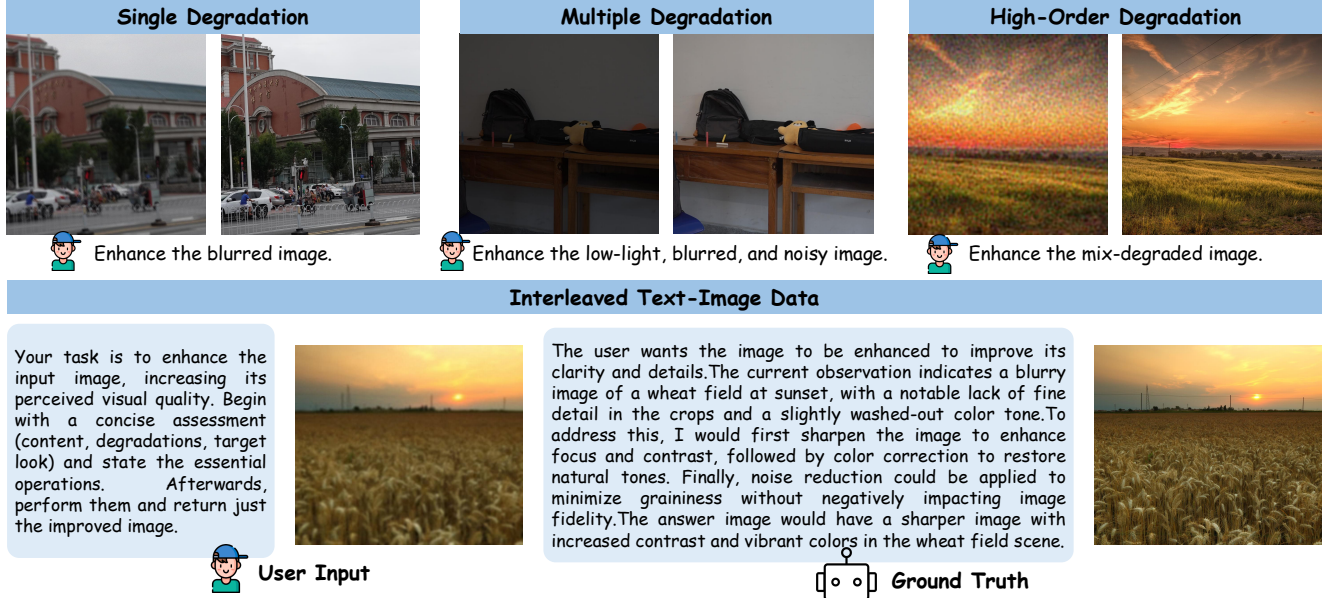


Figure A.2. Data examples for restoration and enhancement training in UARE, covering single, multiple, and high-order degradations as well as interleaved text-image pairs.

Table A.1. Training recipe of UARE.

	single deg.	multi deg.	high-order deg.	Uni ft.
Hyperparameters				
Learning rate		2×10^{-5}		
LR scheduler		Constant		
Weight decay		0.0		
Gradient norm clip		1.0		
Optimizer		AdamW ($\beta_1 = 0.9, \beta_2 = 0.95, \epsilon = 1.0 \times 10^{-15}$)		
Loss weight (CE : MSE)	-	-	-	0.25 : 1
Warm-up steps	250	250	250	500
Training steps	10K	20K	1.5k	10K
EMA ratio	0.990	0.995	0.995	0.995
Training seen tokens	9.6B	19.2B	1.3B	4.6B
Res. resolution (min short side, max long side)		(512, 1024)		
IQA resolution (min short side, max long side)		(378, 980)		
Diffusion timestep shift		4.0		
Data sampling ratio				
IQA	0.0	0.0	0.0	0.25
Single degradation	1.0	0.0	0.0	0.05
Multiple degradation	0.0	1.0	0.0	0.1
high-order degradation	0.0	0.0	1.0	0.2
Interleaved IQA and restoration	0.0	0.0	0.0	0.4

and DIV2K [1]. We compare UARE with **twelve** SR methods: Real-ESRGAN [79], FeMASR [7], SwinIR [45], InvSR [104], StableSR [77], DiffBIR [49], SeeSR [93], PASD [98], ResShift [103], SinSR [82], OSEDiff [92], S3Diff [106], and PURE [85]. The evaluation metrics fol-

low the main paper: for reference-based fidelity, we report PSNR and SSIM [83] on the Y channel in YCbCr space; for reference-based perceptual quality, we use LPIPS and DISTS; for no-reference quality, we adopt NIQE [110], LIQE [112], MUSIQ [34], MANIQA [97], and TOPIQ [8].

Table B.1. Quantitative comparison of different methods on RealSR, DRealSR, and DIV2K. Throughout this paper, best, second-best, and third-best results are highlighted in **bold red**, underlined blue, *italic green*. \uparrow / \downarrow indicate higher/lower is better.

Test Dataset	Method	PSNR \uparrow	SSIM \uparrow	LPIPS \downarrow	DISTS \downarrow	NIQE \downarrow	LIQE \uparrow	MUSIQ \uparrow	MANIQA \uparrow	TOPIQ \uparrow
RealSR	Real-ESRGAN [79]	23.62	<i>0.7185</i>	0.2763	0.2063	5.7619	3.3163	59.87	0.3749	0.5097
	FeMASR [7]	23.26	0.7030	0.2850	0.2254	5.7053	3.1587	58.05	0.3435	0.4848
	SwinIR [45]	23.75	0.7250	0.2608	<i>0.1981</i>	5.6989	3.0798	58.95	0.3546	0.4816
	InvSR [104]	22.90	0.6844	<u>0.2634</u>	<u>0.1980</u>	5.9996	3.7639	67.20	0.4270	0.5546
	StableSR [77]	23.73	0.6979	0.2792	0.2023	5.5914	3.0532	61.65	0.3826	0.5201
	DiffBIR [49]	23.20	0.6346	0.3350	0.2162	4.5879	3.5529	65.25	0.4620	0.6033
	SeeSR [93]	<u>24.34</u>	<u>0.7187</u>	0.2754	0.2134	6.4146	3.3938	65.53	<i>0.4856</i>	0.6246
	PASD [98]	24.50	0.7115	<i>0.2716</i>	0.1954	6.0067	2.8541	58.52	0.3831	0.4969
	ResShift [103]	<i>24.17</i>	0.6528	0.4336	0.2812	8.6273	2.6610	53.38	0.3412	0.4210
	SinSR [82]	23.68	0.6649	0.3490	0.2445	6.5101	3.2255	61.03	0.4230	0.5383
	OSDiff [92]	23.07	0.6850	0.2941	0.2109	5.5054	4.0681	<u>68.95</u>	<u>0.4876</u>	<u>0.6441</u>
	S3Diff [106]	23.16	0.6810	0.2748	0.1986	<i>5.3003</i>	<i>4.0080</i>	<i>67.57</i>	0.4677	<i>0.6301</i>
	PURE [85]	21.31	0.5738	0.3859	0.2468	5.6419	3.7881	66.57	0.4829	<i>0.6301</i>
	UARE (Ours)	21.38	0.6464	0.3095	0.2344	<u>5.2981</u>	<u>4.0658</u>	69.67	0.5260	0.6796
DRealSR	Real-ESRGAN [79]	27.26	<i>0.7745</i>	0.2841	<i>0.2085</i>	6.6994	2.8595	53.43	0.3438	0.4559
	FeMASR [7]	25.32	0.7221	0.3164	0.2241	<u>5.8831</u>	2.9538	53.32	0.3169	0.4722
	SwinIR [45]	27.01	0.7703	<u>0.2793</u>	<u>0.2070</u>	6.5370	2.8340	52.42	0.3310	0.4484
	InvSR [104]	25.55	0.7087	0.3188	0.2192	6.0231	<i>3.7525</i>	<i>64.25</i>	0.4301	0.5726
	StableSR [77]	28.28	0.7981	0.2687	0.2026	7.2816	2.5068	51.62	0.3226	0.4355
	DiffBIR [49]	26.08	0.6578	0.4144	0.2564	4.4856	3.3993	61.81	0.4612	0.6084
	SeeSR [93]	<i>28.14</i>	<u>0.7798</u>	<i>0.2832</i>	0.2241	7.4833	2.7943	55.89	0.3976	0.5436
	PASD [98]	<u>28.18</u>	0.7722	0.2970	0.2108	7.4421	2.6129	51.42	0.3595	0.4587
	ResShift [103]	27.39	0.6907	0.4996	0.3077	9.1788	1.7905	40.58	0.2457	0.3414
	SinSR [82]	26.72	0.6933	0.4031	0.2624	6.8825	2.7781	53.36	0.3677	0.4959
	OSDiff [92]	25.60	0.7403	0.3088	0.2158	6.1544	<u>3.9797</u>	<u>65.24</u>	<u>0.4879</u>	<u>0.6273</u>
	S3Diff [106]	26.18	0.7197	0.3161	0.2099	<i>5.9531</i>	3.9255	63.34	<i>0.4635</i>	<i>0.6181</i>
	PURE [85]	23.04	0.5718	0.4461	0.2674	6.3939	3.7390	60.68	0.4362	0.5888
	UARE (Ours)	21.31	0.5736	0.4071	0.2613	6.4290	4.0445	67.71	0.5121	0.6652
DIV2K	Real-ESRGAN [79]	<u>19.41</u>	<u>0.4901</u>	0.4123	0.2586	4.5100	3.6731	61.63	0.3835	0.5449
	FeMASR [7]	18.46	0.4339	0.4139	0.2382	<i>4.1173</i>	3.4794	61.01	0.3068	0.5151
	SwinIR [45]	19.11	<i>0.4772</i>	0.4285	0.2647	4.7146	3.2109	58.22	0.3251	0.4844
	InvSR [104]	18.93	0.4597	0.4182	0.2685	5.8936	3.5459	61.91	0.4066	0.5573
	StableSR [77]	19.85	0.4940	0.4796	0.2887	5.7479	1.8466	43.25	0.2181	0.3276
	DiffBIR [49]	18.94	0.4332	0.4009	0.2238	3.6594	3.8573	67.20	0.4574	0.6467
	SeeSR [93]	19.11	0.4580	<i>0.3769</i>	0.2339	4.5817	3.7445	66.31	<i>0.4686</i>	0.6330
	PASD [98]	18.98	0.4562	0.4293	0.2373	4.7846	3.6022	63.46	0.4025	0.5653
	ResShift [103]	<i>19.15</i>	0.4311	0.4900	0.2808	7.4321	2.8862	56.02	0.3534	0.4662
	SinSR [82]	18.58	0.4059	0.4483	0.2455	6.0533	3.4629	64.12	0.4483	0.5997
	OSDiff [92]	18.86	0.4563	<u>0.3579</u>	<i>0.2209</i>	4.1756	3.8877	67.83	0.4422	0.6269
	S3Diff [106]	18.76	0.4490	0.3299	0.1990	4.2026	<u>4.2692</u>	<i>69.31</i>	0.4675	<u>0.6679</u>
	PURE [85]	16.71	0.3661	0.4449	0.2293	4.9545	4.2701	<u>70.06</u>	0.5201	<i>0.6621</i>
	UARE (Ours)	16.59	0.3857	0.4074	<u>0.2138</u>	<u>3.7931</u>	<i>4.2627</i>	70.45	<u>0.5028</u>	0.6864

As shown in Tab. B.1, UARE achieves higher SSIM and lower LPIPS/DISTS than PURE, and clearly outperforms all competing methods on MUSIQ, MANIQA, and TOPIQ, while ranking second-best on NIQE and LIQE. These results confirm that UARE delivers the best overall perceptual

quality among all compared methods.

Additionally, we evaluate UARE on RealSet80 [103], which contains 80 low-resolution real-world images without ground-truth references. We compare UARE against BSRGAN, StableSR, DiffBIR, SeeSR, SinSR, OSDiff,

Table B.2. Quantitative comparison of different methods on RealSet80 without ground truth.

Method	NIQE↓	LIQE↑	MUSIQ↑	MANIQA↑	TOPIQ↑
BSRGAN [108]	5.1655	3.8884	64.85	0.3941	0.5821
StableSR [77]	4.0798	3.9074	67.67	0.4682	0.6440
DiffBIR [49]	6.1069	4.1113	68.10	0.5527	0.6736
SeeSR [93]	5.2244	4.3317	69.70	0.5362	0.6887
SinSR [82]	6.4250	3.6613	62.78	0.4483	0.5854
OSDiff [92]	4.6362	4.2251	68.88	0.4995	0.6062
PURE [85]	5.3617	4.2528	69.55	0.5215	0.6647
UARE (Ours)	4.6044	4.1804	70.05	0.5363	0.6446

Table B.3. Quantitative comparison of different methods on four single-degradation subset of FoundIR. For each method, the first row lists PSNR/LPIPS and the second row lists NIQE/MANIQA.

Method	Blur	Haze	RainDrop	Lowlight
Restormer [105]	21.53 / 0.3821 6.9553 / 0.1322	13.70 / 0.5687 5.6395 / 0.2695	24.63 / 0.3029 5.0340 / 0.2777	9.20 / 0.6037 7.3095 / 0.2207
PromptIR [65]	21.64 / 0.4041 8.0897 / 0.1361	18.31 / 0.4762 5.7593 / 0.2815	26.67 / 0.2203 4.8115 / 0.2449	16.67 / 0.4804 7.7780 / 0.2317
DiffIR [49]	21.61 / 0.3823 7.4800 / 0.1390	19.78 / 0.2345 3.4547 / 0.3235	26.19 / 0.2367 3.2762 / 0.2593	18.05 / 0.3146 4.9243 / 0.2828
DiffUIR [119]	26.99 / 0.1912 6.1600 / 0.2734	20.50 / 0.2037 3.7435 / 0.3540	29.52 / 0.1292 4.0766 / 0.2697	14.88 / 0.2691 6.0439 / 0.3615
SUPIR [102]	20.63 / 0.3180 4.8374 / 0.2702	13.66 / 0.3883 3.8944 / 0.3482	21.41 / 0.3552 4.7940 / 0.2933	7.43 / 0.6460 7.6004 / 0.2680
InstructIR [13]	19.81 / 0.2335 6.1392 / 0.2394	17.27 / 0.2267 3.4979 / 0.3663	21.75 / 0.3456 4.7295 / 0.2935	20.78 / 0.2473 4.9299 / 0.3184
AutoDIR [32]	19.98 / 0.3400 6.8772 / 0.1652	15.59 / 0.4130 4.9741 / 0.2909	21.46 / 0.3643 5.2210 / 0.2836	22.36 / 0.3487 7.6178 / 0.2567
FoundIR [42]	26.10 / 0.1709 5.6797 / 0.2854	23.29 / 0.1896 3.9543 / 0.3544	30.86 / 0.0897 4.3657 / 0.2793	20.34 / 0.2499 6.7511 / 0.3460
UARE (Ours)	22.38 / 0.1904 4.7313 / 0.3361	21.28 / 0.1635 3.2674 / 0.4232	28.26 / 0.0981 4.6515 / 0.3008	19.64 / 0.1841 5.0119 / 0.4234

and PURE using five no-reference image quality metrics: NIQE, LIQE, MUSIQ, MANIQA, and TOPIQ. As reported in Tab. B.2, UARE ranks first on MUSIQ and second on NIQE and MANIQA, further demonstrating its effectiveness in challenging real-world scenarios.

More qualitative comparisons. Figs. B.1, B.2, B.3 and B.4 present visual comparisons across super-resolution images produced by these approaches. It can be seen that our method effectively restores fine image details, such as knots, text, and petals, while producing noticeably fewer artifacts. These results comprehensively confirm the effectiveness of UARE in image super-resolution.

B.2. Image Restoration and Enhancement

More quantitative results. We have reported the restoration/enhancement results on the multi-degradation subsets of FoundIR [42] in the main paper. Here, we further compare UARE with Restormer [105], PromptIR [65], DiffIR [95], DiffUIR [119], SUPIR [102], InstructIR [13], AutoDIR [32], and FoundIR [42] on the single-degradation subsets of FoundIR, including blur, haze, raindrop, and low-

Table B.4. User study results of different SR methods.

Method	OSDiff	S3Diff	PURE	UARE (Ours)
Total Votes	25	48	31	186
Voting Rate (%)	8.62	16.55	10.69	64.14

Table B.5. User study results of different restoration methods.

Method	DiffIR	DiffUIR	FoundIR	UARE (Ours)
Total Votes	5	15	20	250
Voting Rate (%)	1.72	5.17	6.90	86.21

light, as shown in Tab. B.3. UARE ranks first in MANIQA across all subsets. In addition, it achieves competitive PSNR, LPIPS, and NIQE results, indicating superior performance and a favorable trade-off between fidelity and perceptual quality.

More qualitative results. Figs. B.5, B.6, B.7, B.8 and B.9 present visual comparison across restored/enhanced images produced by these approaches. It can be seen that UARE faithfully reconstructs challenging details, such as text in blurred or low-light regions, hair, and the fine structures of flowers and vegetation. These results comprehensively confirm the effectiveness of UARE across multiple image restoration and enhancement tasks.

B.3. User Study

To further evaluate the effectiveness of our UARE, we conduct a user study comparing four SR and restoration methods, respectively. We employ ten LR images from the RealSR, DRealSR and DIV2K datasets, and ten LQ images from the FoundIR test set. Compared SR methods include OSDiff [92], S3Diff [106] and PURE [85], while restoration methods include DiffIR [95], DiffUIR [119] and FoundIR [42]. Twenty-nine expert researchers are invited to choose the best super-resolution/restored image for each test sample based on two equally weighted criteria: (1) perceptual quality, focusing on clarity, detail, and realism, and (2) content consistency with the LR/LQ input, including alignment in image structure and texture.

As reported in Tab. B.4, UARE achieves a high voting rate of 64.14% in comparison with SR methods, which is significant better preference than other methods. Besides, as shown in Tab. B.5, UARE achieves a voting rate of 86.21% in comparison of different all-in-one restoration methods. These results show that users overwhelmingly prefer UARE over both SR and restoration baselines. In particular, UARE receives nearly four times as many votes as the best competing SR method and more than an order of magnitude more votes than the strongest all-in-one restoration baseline. These consistent user preferences demonstrate that UARE achieves a better balance between perceptual quality and content fidelity, as well as our unified

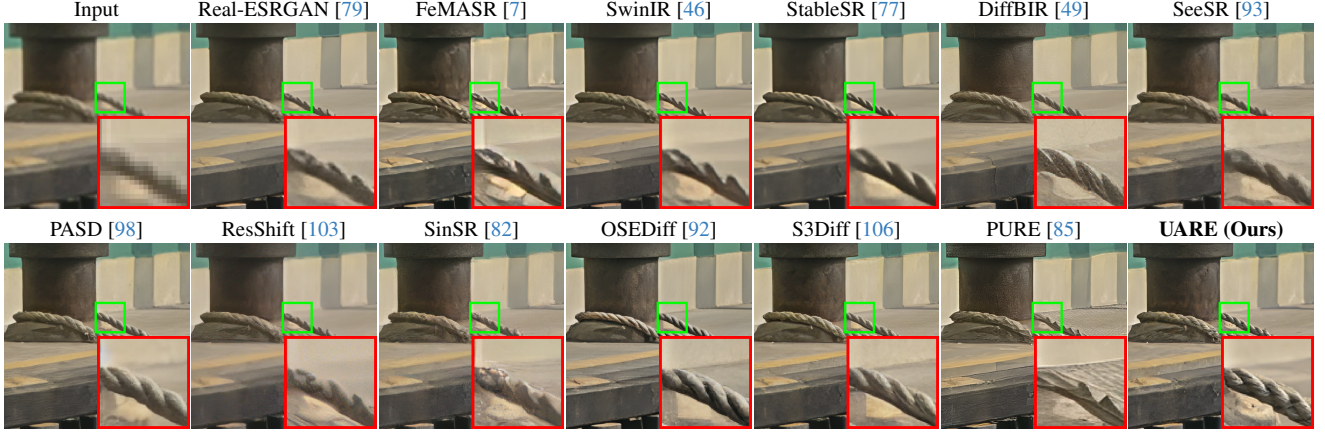


Figure B.1. Visual comparison on the image named “Canon_043” from the RealSR dataset.

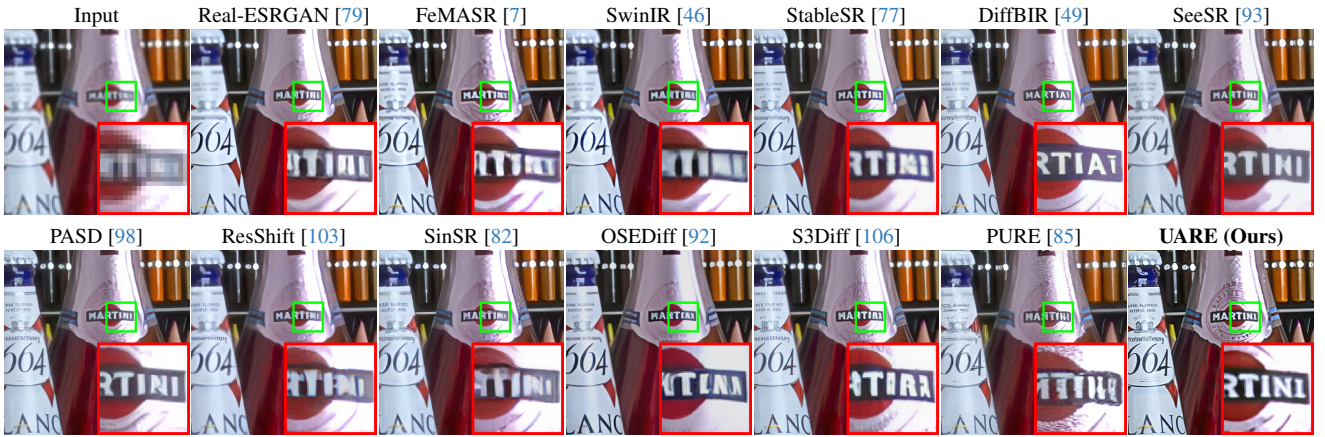


Figure B.2. Visual comparison on the image named “Canon_050” from the RealSR dataset.

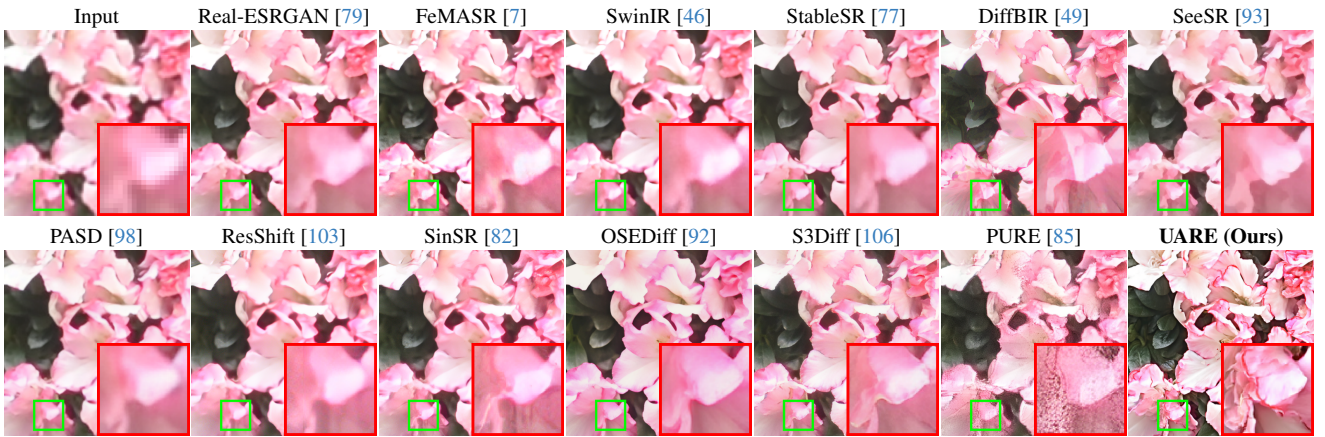


Figure B.3. Visual comparison on the image named “DSC_1425_x1” from the DRealSR dataset.

IQA-and-restoration scheme.

C. Discussion and Limitations

Due to the large number of parameters in the unified model, UARE has a relatively large model size and slow inference

speed, which limits its deployment on resource-constrained devices. In addition, although we demonstrate that IQA can boost restoration and enhancement performance, how restoration and enhancement, in turn, can better improve IQA remains an open question and requires further study.

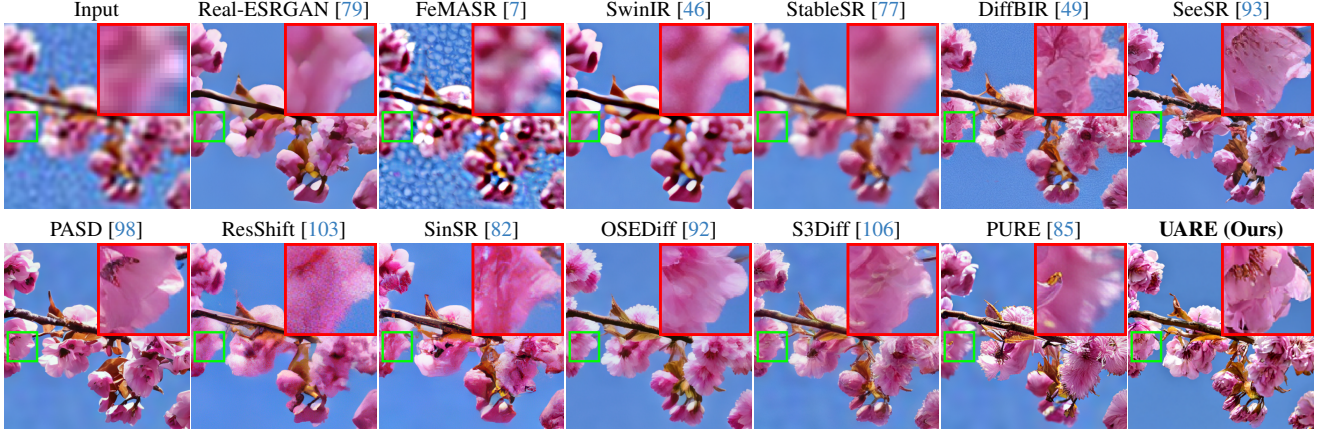


Figure B.4. Visual comparison on the image named “0000098” from the DIV2K dataset.

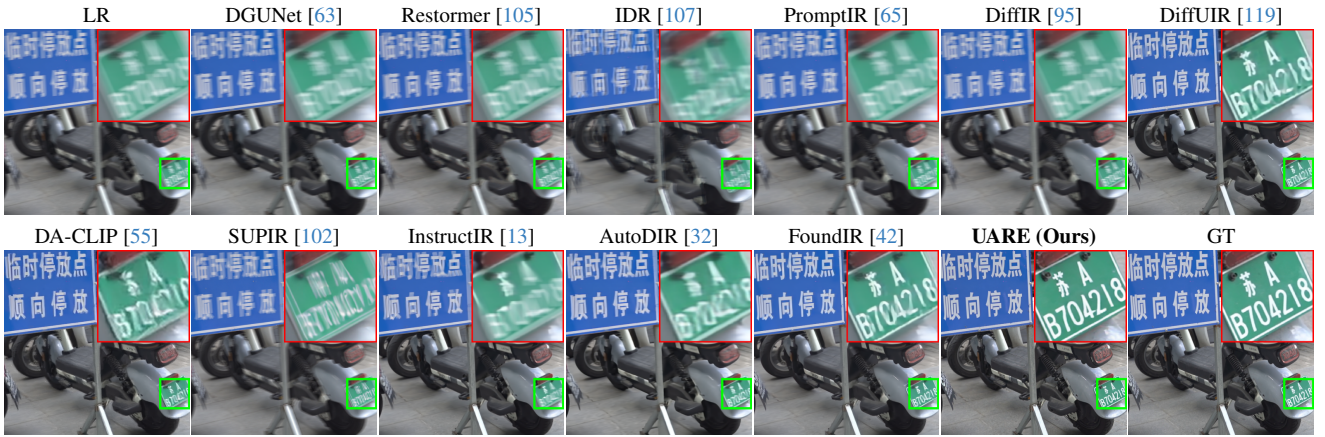


Figure B.5. Visual comparison on the image “0131” with blur from the FoundIR dataset.

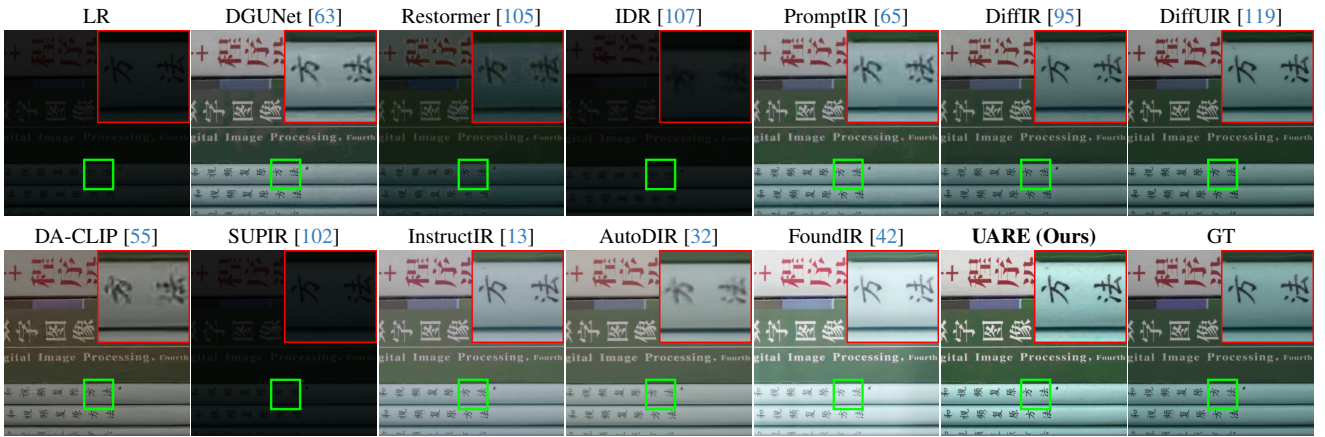


Figure B.6. Visual comparison on the image “1143” with low-light from the FoundIR dataset.

References

- [1] Eirikur Agustsson and Radu Timofte. Ntire 2017 challenge on single image super-resolution: Dataset and study. In *Proceedings of the IEEE/CVF Conference on Computer Vision and Pattern Recognition Workshops (CVPRW)*, pages 126–135, 2017. [7](#), [10](#)
- [2] Yang Ai, Huaibo Huang, Xiaoqiang Zhou, Jiexiang Wang, and Ran He. Multimodal prompt perceiver: Empower adaptiveness generalizability and fidelity for all-in-one image restoration. In *Proceedings of the IEEE/CVF Conference on Computer Vision and Pattern Recognition (CVPR)*, 2024. [3](#)

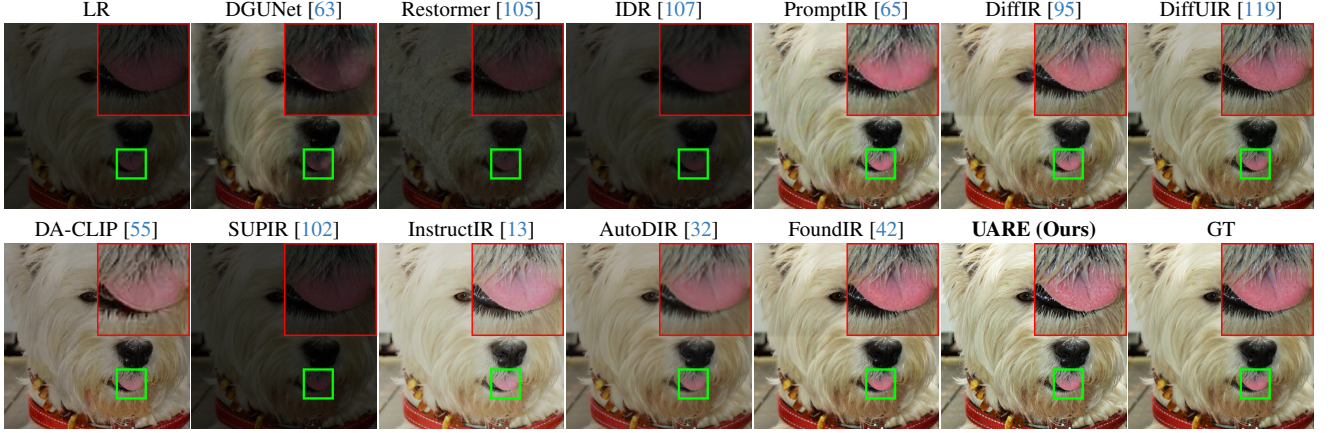


Figure B.7. Visual comparison on the image “1304” with low-light and JPEG compression from the FoundIR dataset.

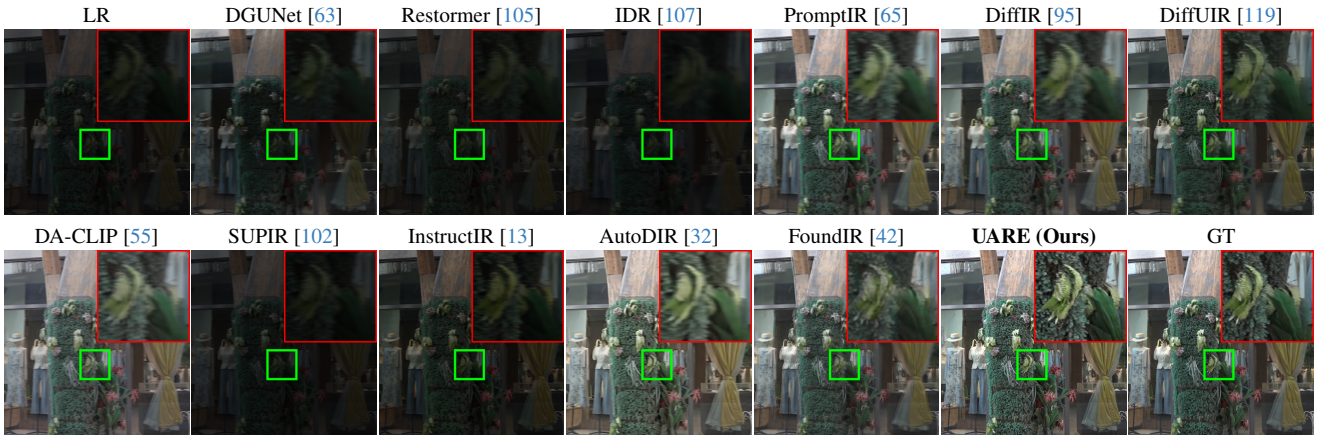


Figure B.8. Visual comparison on the image “1397” with low-light, blur and noise from the FoundIR dataset.

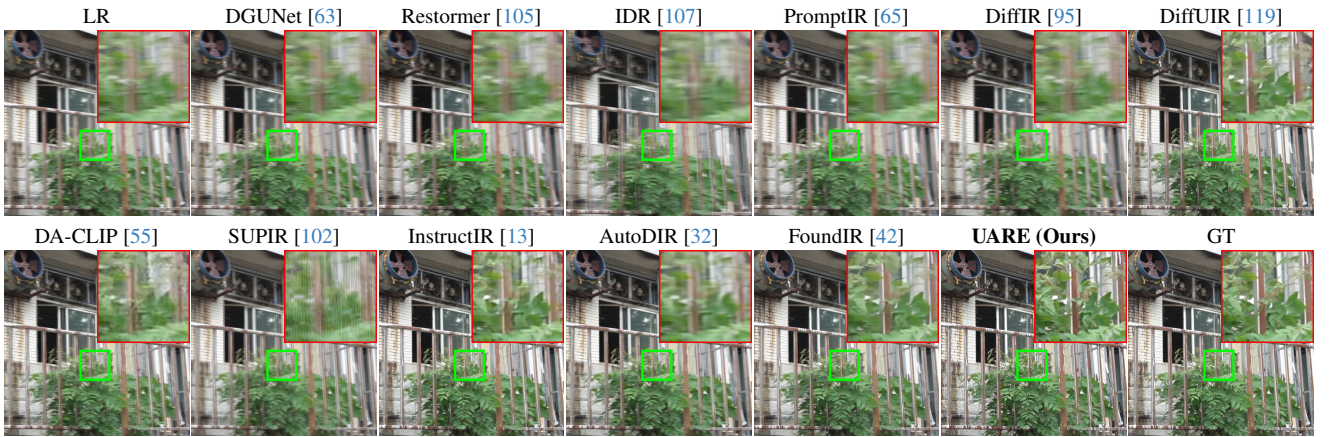


Figure B.9. Visual comparison on the image “0243” with blur and JPEG compression from the FoundIR dataset.

- [3] Sebastian Bosse, Dominique Maniry, Klaus-Robert Müller, Thomas Wiegand, and Wojciech Samek. Deep neural networks for no-reference and full-reference image quality assessment. *IEEE Transactions on Image Processing (TIP)*, 27(1):206–219, 2017. 2

- [4] Jianrui Cai, Hui Zeng, Hongwei Yong, Zisheng Cao,

- and Lei Zhang. Toward real-world single image super-resolution: A new benchmark and a new model. In *Proceedings of the IEEE/CVF Conference on Computer Vision and Pattern Recognition (CVPR)*, pages 3086–3095, 2019. 7, 9

- [5] Shuo Cao, Yihao Liu, Wenlong Zhang, Yu Qiao, and Chao

- Dong. Grids: Grouped multiple-degradation restoration with image degradation similarity. In *Proceedings of the European Conference on Computer Vision (ECCV)*, 2024. 3
- [6] Yue Cao, Zhaolin Wan, Dongwei Ren, Zifei Yan, and Wangmeng Zuo. Incorporating semi-supervised and positive-unlabeled learning for boosting full reference image quality assessment. In *Proceedings of the IEEE/CVF Conference on Computer Vision and Pattern Recognition (CVPR)*, pages 5851–5861, 2022. 2
- [7] Chaofeng Chen, Xinyu Shi, Yipeng Qin, Xiaoming Li, Xiaoguang Han, Tao Yang, and Shihui Guo. Real-world blind super-resolution via feature matching with implicit high-resolution priors. In *Proceedings of the ACM International Conference on Multimedia (ACM MM)*, pages 1329–1338, 2022. 3, 10, 11, 13, 14
- [8] Chaofeng Chen, Jiadi Mo, Jingwen Hou, Haoning Wu, Liang Liao, Wenxiu Sun, Qiong Yan, and Weisi Lin. Topiq: A top-down approach from semantics to distortions for image quality assessment. *IEEE Transactions on Image Processing (TIP)*, 33:2404–2418, 2024. 7, 10
- [9] Chaofeng Chen, Sensen Yang, Haoning Wu, Liang Liao, Zicheng Zhang, Annan Wang, Wenxiu Sun, Qiong Yan, and Weisi Lin. Q-ground: Image quality grounding with large multi-modality models. In *Proceedings of the ACM International Conference on Multimedia (ACM MM)*, pages 486–495, 2024. 3
- [10] Du Chen, Tianhe Wu, Kede Ma, and Lei Zhang. Toward generalized image quality assessment: Relaxing the perfect reference quality assumption. In *Proceedings of the IEEE/CVF Conference on Computer Vision and Pattern Recognition (CVPR)*, 2025. 4
- [11] Jiuhai Chen, Zhiyang Xu, Xichen Pan, Yushi Hu, Can Qin, Tom Goldstein, Lifu Huang, Tianyi Zhou, Saining Xie, Silvio Savarese, et al. Blip3-o: A family of fully open unified multimodal models-architecture, training and dataset. *arXiv preprint arXiv:2505.09568*, 2025. 3
- [12] Xiaokang Chen, Zhiyu Wu, Xingchao Liu, Zizheng Pan, Wen Liu, Zhenda Xie, Xingkai Yu, and Chong Ruan. Janus-pro: Unified multimodal understanding and generation with data and model scaling. *arXiv preprint arXiv:2501.17811*, 2025. 3
- [13] Marcos V Conde, Gregor Geigle, and Radu Timofte. Instructir: High-quality image restoration following human instructions. In *Proceedings of the European Conference on Computer Vision (ECCV)*, 2024. 7, 8, 12, 14, 15
- [14] Mostafa Dehghani, Basil Mustafa, Josip Djolonga, Jonathan Heek, Matthias Minderer, Mathilde Caron, Andreas Steiner, Joan Puigcerver, Robert Geirhos, Ibrahim M Alabdulmohsin, et al. Patch n’pack: Navit, a vision transformer for any aspect ratio and resolution. *Proceedings of the Advances in Neural Information Processing Systems (NeurIPS)*, 36:2252–2274, 2023. 6
- [15] Chaorui Deng, Deyao Zhu, Kunchang Li, Chenhui Gou, Feng Li, Zeyu Wang, Shu Zhong, Weihao Yu, Xiaonan Nie, Ziang Song, Guang Shi, and Haoqi Fan. Emerging properties in unified multimodal pretraining. *arXiv preprint arXiv:2505.14683*, 2025. 2, 3, 4, 6
- [16] Senyou Deng, Wenqi Ren, Yanyang Yan, Tao Wang, Fenglong Song, and Xiaochun Cao. Multi-scale separable network for ultra-high-definition video deblurring. In *Proceedings of the IEEE/CVF International Conference on Computer Vision (ICCV)*, 2021. 3
- [17] Prafulla Dhariwal and Alexander Nichol. Diffusion models beat gans on image synthesis. *Proceedings of the Advances in Neural Information Processing Systems (NeurIPS)*, 34: 8780–8794, 2021. 3
- [18] Keyan Ding, Kede Ma, Shiqi Wang, and Eero P Simoncelli. Image quality assessment: Unifying structure and texture similarity. *IEEE Transactions on Pattern Analysis and Machine Intelligence (TPAMI)*, 44(5):2567–2581, 2020. 2
- [19] Keyan Ding, Yi Liu, Xueyi Zou, Shiqi Wang, and Kede Ma. Locally adaptive structure and texture similarity for image quality assessment. In *Proceedings of the ACM International Conference on Multimedia (ACM MM)*, pages 2483–2491, 2021. 2
- [20] Chao Dong, Chen Change Loy, Kaiming He, and Xiaoou Tang. Learning a deep convolutional network for image super-resolution. In *Proceedings of the European Conference on Computer Vision (ECCV)*, pages 184–199. Springer, 2014. 2
- [21] Patrick Esser, Sumith Kulal, Andreas Blattmann, Rahim Entezari, Jonas Müller, Harry Saini, Yam Levi, Dominik Lorenz, Axel Sauer, Frederic Boesel, et al. Scaling rectified flow transformers for high-resolution image synthesis. In *Proceedings of the International Conference on Machine Learning (ICML)*, 2024. 6
- [22] Yuming Fang, Hanwei Zhu, Yan Zeng, Kede Ma, and Zhou Wang. Perceptual quality assessment of smartphone photography. In *Proceedings of the IEEE/CVF Conference on Computer Vision and Pattern Recognition (CVPR)*, pages 3677–3686, 2020. 4, 8
- [23] Deepti Ghadiyaram and Alan C Bovik. Live in the wild image quality challenge database. *Online: <http://live.ece.utexas.edu/research/ChallengeDB/index.html>* [Mar, 2017], 2015. 8
- [24] Abhijay Ghildyal and Feng Liu. Shift-tolerant perceptual similarity metric. In *Proceedings of the European Conference on Computer Vision (ECCV)*, pages 91–107. Springer, 2022. 2
- [25] Jinjin GU, Haoming Cai, Haoyu Chen, Xiaoxing Ye, Ren Jimmy S, and Chao Dong. Pipal: a large-scale image quality assessment dataset for perceptual image restoration. In *Proceedings of the European Conference on Computer Vision (ECCV)*, pages 633–651. Springer, 2020. 4
- [26] Yu Guo, Yuan Gao, Yuxu Lu, Huilin Zhu, Ryan Wen Liu, and Shengfeng He. Onerestore: A universal restoration framework for composite degradation. In *Proceedings of the European Conference on Computer Vision (ECCV)*, 2024. 3
- [27] Jonathan Ho and Tim Salimans. Classifier-free diffusion guidance. *arXiv preprint arXiv:2207.12598*, 2022. 6
- [28] Vlad Hosu, Hanhe Lin, Tamas Sziranyi, and Dietmar Saupe. Koniq-10k: An ecologically valid database for deep learning of blind image quality assessment. *IEEE Trans-*

- actions on Image Processing (TIP), 29:4041–4056, 2020. 4
- [29] Jia-Bin Huang, Abhishek Singh, and Narendra Ahuja. Single image super-resolution from transformed self-exemplars. In *Proceedings of the IEEE/CVF Conference on Computer Vision and Pattern Recognition (CVPR)*, 2015. 3
 - [30] Runhui Huang, Chunwei Wang, Junwei Yang, Guansong Lu, Yunlong Yuan, Jianhua Han, Lu Hou, Wei Zhang, Lanqing Hong, Hengshuang Zhao, et al. Illume+: Illuminating unified mllm with dual visual tokenization and diffusion refinement. *arXiv preprint arXiv:2504.01934*, 2025. 3
 - [31] Kui Jiang, Zhongyuan Wang, Peng Yi, Chen Chen, Baojin Huang, Yimin Luo, Jiayi Ma, and Junjun Jiang. Multi-scale progressive fusion network for single image deraining. In *Proceedings of the IEEE/CVF Conference on Computer Vision and Pattern Recognition (CVPR)*, 2020. 3
 - [32] Yitong Jiang, Zhaoyang Zhang, Tianfan Xue, and Jinwei Gu. Autodir: Automatic all-in-one image restoration with latent diffusion. In *Proceedings of the European Conference on Computer Vision (ECCV)*, 2024. 7, 8, 12, 14, 15
 - [33] Le Kang, Peng Ye, Yi Li, and David Doermann. Convolutional neural networks for no-reference image quality assessment. In *Proceedings of the IEEE/CVF Conference on Computer Vision and Pattern Recognition (CVPR)*, pages 1733–1740, 2014. 3
 - [34] Junjie Ke, Qifei Wang, Yilin Wang, Peyman Milanfar, and Feng Yang. Musiq: Multi-scale image quality transformer. In *Proceedings of the IEEE/CVF International Conference on Computer Vision (ICCV)*, pages 5148–5157, 2021. 3, 7, 8, 10
 - [35] Diederik P Kingma and Max Welling. Auto-encoding variational bayes. *arXiv preprint arXiv:1312.6114*, 2013. 4
 - [36] Xiangtao Kong, Chao Dong, and Lei Zhang. Towards effective multiple-in-one image restoration: A sequential and prompt learning strategy. *arXiv preprint arXiv:2401.03379*, 2024. 3
 - [37] Black Forest Labs. Flux. <https://github.com/black-forest-labs/flux>, 2024. 6
 - [38] Eric C Larson and Damon M Chandler. Most apparent distortion: full-reference image quality assessment and the role of strategy. *Journal of Electronic Imaging*, 19(1): 011006–011006, 2010. 8
 - [39] Christian Ledig, Lucas Theis, Ferenc Huszár, Jose Caballero, Andrew Cunningham, Alejandro Acosta, Andrew Aitken, Alykhan Tejani, Johannes Totz, Zehan Wang, et al. Photo-realistic single image super-resolution using a generative adversarial network. In *Proceedings of the IEEE/CVF Conference on Computer Vision and Pattern Recognition (CVPR)*, pages 4681–4690, 2017. 2
 - [40] Chongyi Li, Chun-Le Guo, Man Zhou, Zhixin Liang, Shangchen Zhou, Ruicheng Feng, and Chen Change Loy. Embedding fourier for ultra-high-definition low-light image enhancement. In *Proceedings of the International Conference on Learning Representations (ICLR)*, 2023. 2, 3
 - [41] Chunyi Li, Zicheng Zhang, Haoning Wu, Wei Sun, Xiongkuo Min, Xiaohong Liu, Guangtao Zhai, and Weisi Lin. Aigqa-3k: An open database for ai-generated image quality assessment. *IEEE Transactions on Circuits and Systems for Video Technology (TCSVT)*, 34(8):6833–6846, 2023. 8
 - [42] Hao Li, Xiang Chen, Jiangxin Dong, Jinhui Tang, and Jinshan Pan. Foundir: Unleashing million-scale training data to advance foundation models for image restoration. In *Proceedings of the IEEE/CVF International Conference on Computer Vision (ICCV)*, 2025. 2, 3, 4, 5, 7, 8, 12, 14, 15
 - [43] Weiqi Li, Xuanyu Zhang, Shijie Zhao, Yabin Zhang, Junlin Li, Li Zhang, and Jian Zhang. Q-insight: Understanding image quality via visual reinforcement learning. *Proceedings of the Advances in Neural Information Processing Systems (NeurIPS)*, 2025. 2, 3, 4, 8
 - [44] Yawei Li, Kai Zhang, Jingyun Liang, Jiezhong Cao, Ce Liu, Rui Gong, Yulun Zhang, Hao Tang, Yun Liu, Denis Demidolx, et al. Lsdir: A large scale dataset for image restoration. In *Proceedings of the IEEE/CVF Conference on Computer Vision and Pattern Recognition Workshops (CVPRW)*, 2023. 5
 - [45] Jingyun Liang, Jiezhong Cao, Guolei Sun, Kai Zhang, Luc Van Gool, and Radu Timofte. Swinir: Image restoration using swin transformer. In *Proceedings of the IEEE/CVF International Conference on Computer Vision (ICCV)*, 2021. 10, 11
 - [46] Jingyun Liang, Jiezhong Cao, Guolei Sun, Kai Zhang, Luc Van Gool, and Radu Timofte. Swinir: Image restoration using swin transformer. In *Proceedings of the IEEE/CVF International Conference on Computer Vision (ICCV)*, pages 1833–1844, 2021. 2, 3, 13, 14
 - [47] Bin Lin, Zongjian Li, Xinhua Cheng, Yuwei Niu, Yang Ye, Xianyi He, Shenghai Yuan, Wangbo Yu, Shaodong Wang, Yongyang Ge, et al. Uniworld: High-resolution semantic encoders for unified visual understanding and generation. *arXiv preprint arXiv:2506.03147*, 2025. 3
 - [48] Hanhe Lin, Vlad Hosu, and Dietmar Saupe. Kadid-10k: A large-scale artificially distorted iqa database. In *Proceedings of International Conference on Quality of Multimedia Experience (QoMEX)*, pages 1–3. IEEE, 2019. 2, 4, 8
 - [49] Xinqi Lin, Jingwen He, Ziyang Chen, Zhaoyang Lyu, Bo Dai, Fanghua Yu, Yu Qiao, Wanli Ouyang, and Chao Dong. Diffbir: Toward blind image restoration with generative diffusion prior. In *Proceedings of the European Conference on Computer Vision (ECCV)*, pages 430–448, 2024. 3, 5, 6, 7, 10, 11, 12, 13, 14
 - [50] Yaron Lipman, Ricky TQ Chen, Heli Ben-Hamu, Maximilian Nickel, and Matt Le. Flow matching for generative modeling. *arXiv preprint arXiv:2210.02747*, 2022. 6
 - [51] Jiawei Liu, Qiang Wang, Huijie Fan, Yinong Wang, Yandong Tang, and Liangqiong Qu. Residual denoising diffusion models. In *Proceedings of the IEEE/CVF Conference on Computer Vision and Pattern Recognition (CVPR)*, pages 2773–2783, 2024. 3
 - [52] Xialei Liu, Joost Van De Weijer, and Andrew D Bagdanov. Rankiqa: Learning from rankings for no-reference image quality assessment. In *Proceedings of the IEEE/CVF International Conference on Computer Vision (ICCV)*, pages 1040–1049, 2017. 3

- [53] Xingchao Liu, Chengyue Gong, and Qiang Liu. Flow straight and fast: Learning to generate and transfer data with rectified flow. *arXiv preprint arXiv:2209.03003*, 2022. 6
- [54] Ilya Loshchilov and Frank Hutter. Decoupled weight decay regularization. *arXiv preprint arXiv:1711.05101*, 2017. 6
- [55] Ziwei Luo, Fredrik K Gustafsson, Zheng Zhao, Jens Sjölund, and Thomas B Schön. Controlling vision-language models for universal image restoration. In *Proceedings of the International Conference on Learning Representations (ICLR)*, 2024. 2, 3, 14, 15
- [56] Chao Ma, Chih-Yuan Yang, Xiaokang Yang, and Ming-Hsuan Yang. Learning a no-reference quality metric for single-image super-resolution. *Computer Vision and Image Understanding*, 158:1–16, 2017. 2
- [57] Yiyang Ma, Xingchao Liu, Xiaokang Chen, Wen Liu, Chengyue Wu, Zhiyu Wu, Zizheng Pan, Zhenda Xie, Haowei Zhang, Liang Zhao, et al. Janusflow: Harmonizing autoregression and rectified flow for unified multimodal understanding and generation. *arXiv preprint arXiv:2411.07975*, 2024. 2
- [58] David Martin, Charless Fowlkes, Doron Tal, and Jitendra Malik. A database of human segmented natural images and its application to evaluating segmentation algorithms and measuring ecological statistics. In *Proceedings of the IEEE/CVF International Conference on Computer Vision (ICCV)*, 2001. 3
- [59] Anish Mittal, Anush Krishna Moorthy, and Alan Conrad Bovik. No-reference image quality assessment in the spatial domain. *IEEE Transactions on Image Processing (TIP)*, 21(12):4695–4708, 2012. 2, 8
- [60] Anish Mittal, Rajiv Soundararajan, and Alan C Bovik. Making a “completely blind” image quality analyzer. *IEEE Signal Processing Letters*, 20(3):209–212, 2012. 8
- [61] Anush Krishna Moorthy and Alan Conrad Bovik. A two-step framework for constructing blind image quality indices. *IEEE Signal Processing Letters*, 17(5):513–516, 2010.
- [62] Anush Krishna Moorthy and Alan Conrad Bovik. Blind image quality assessment: From natural scene statistics to perceptual quality. *IEEE Transactions on Image Processing (TIP)*, 20(12):3350–3364, 2011. 2
- [63] Chong Mou, Qian Wang, and Jian Zhang. Deep generalized unfolding networks for image restoration. In *Proceedings of the IEEE/CVF Conference on Computer Vision and Pattern Recognition (CVPR)*, 2022. 2, 3, 14, 15
- [64] Da Pan, Ping Shi, Ming Hou, Zefeng Ying, Sizhe Fu, and Yuan Zhang. Blind predicting similar quality map for image quality assessment. In *Proceedings of the IEEE/CVF Conference on Computer Vision and Pattern Recognition (CVPR)*, pages 6373–6382, 2018. 3
- [65] Vaishnav Potlapalli, Syed Waqas Zamir, Salman H Khan, and Fahad Shahbaz Khan. Promptir: Prompting for all-in-one image restoration. In *Proceedings of the Advances in Neural Information Processing Systems (NeurIPS)*, 2024. 2, 3, 7, 8, 12, 14, 15
- [66] Ekta Prashnani, Hong Cai, Yasamin Mostofi, and Pradeep Sen. Picapp: Perceptual image-error assessment through pairwise preference. In *Proceedings of the IEEE/CVF Conference on Computer Vision and Pattern Recognition (CVPR)*, pages 1808–1817, 2018. 2
- [67] Michele A Saad, Alan C Bovik, and Christophe Charrier. Blind image quality assessment: A natural scene statistics approach in the dct domain. *IEEE Transactions on Image Processing (TIP)*, 21(8):3339–3352, 2012. 2
- [68] Hamid R Sheikh and Alan C Bovik. Image information and visual quality. *IEEE Transactions on Image Processing (TIP)*, 15(2):430–444, 2006. 2
- [69] Shaolin Su, Qingsen Yan, Yu Zhu, Cheng Zhang, Xin Ge, Jinqiu Sun, and Yanning Zhang. Blindly assess image quality in the wild guided by a self-adaptive hyper network. In *Proceedings of the IEEE/CVF Conference on Computer Vision and Pattern Recognition (CVPR)*, pages 3667–3676, 2020. 3
- [70] Simeng Sun, Tao Yu, Jiahua Xu, Wei Zhou, and Zhibo Chen. Graphiq: Learning distortion graph representations for blind image quality assessment. *IEEE Transactions on Multimedia (TMM)*, 25:2912–2925, 2022. 3
- [71] Chameleon Team. Chameleon: Mixed-modal early-fusion foundation models. *arXiv preprint arXiv:2405.09-818*, 2024. 2, 3
- [72] Radu Timofte, Vincent De Smet, and Luc Van Gool. A+: Adjusted anchored neighborhood regression for fast super-resolution. In *Proceedings of the Asian Conference on Computer Vision (ACCV)*, pages 111–126. Springer, 2015. 2
- [73] Shengbang Tong, David Fan, Jiachen Zhu, Yunyang Xiong, Xinlei Chen, Koustuv Sinha, Michael Rabbat, Yann LeCun, Saining Xie, and Zhuang Liu. Metamorph: Multimodal understanding and generation via instruction tuning. *arXiv preprint arXiv:2412.14164*, 2024. 2, 3
- [74] Michael Tschannen, Alexey Gritsenko, Xiao Wang, Muhammad Ferjad Naeem, Ibrahim Alabdulmohsin, Nikhil Parthasarathy, Talfan Evans, Lucas Beyer, Ye Xia, Basil Mustafa, et al. Siglip 2: Multilingual vision-language encoders with improved semantic understanding, localization, and dense features. *arXiv preprint arXiv:2502.14786*, 2025. 4
- [75] Boyang Wang, Fengyu Yang, Xihang Yu, Chao Zhang, and Hanbin Zhao. Apisr: Anime production inspired real-world anime super-resolution. In *Proceedings of the IEEE/CVF Conference on Computer Vision and Pattern Recognition (CVPR)*, pages 25574–25584, 2024. 2, 5
- [76] Chunwei Wang, Guansong Lu, Junwei Yang, Runhui Huang, Jianhua Han, Lu Hou, Wei Zhang, and Hang Xu. Illume: Illuminating your llms to see, draw, and self-enhance. *arXiv preprint arXiv:2412.06673*, 2024. 3
- [77] Jianyi Wang, Zongsheng Yue, Shangchen Zhou, Kelvin CK Chan, and Chen Change Loy. Exploiting diffusion prior for real-world image super-resolution. *International Journal of Computer Vision (IJCV)*, 132(12):5929–5949, 2024. 2, 3, 5, 6, 7, 8, 10, 11, 12, 13, 14
- [78] Wenjing Wang, Huan Yang, Jianlong Fu, and Jiaying Liu. Zero-reference low-light enhancement via physical quadruple priors. In *Proceedings of the IEEE/CVF Conference on*

Computer Vision and Pattern Recognition (CVPR), 2024. 2, 3

- [79] Xintao Wang, Liangbin Xie, Chao Dong, and Ying Shan. Real-esrgan: Training real-world blind super-resolution with pure synthetic data. In *Proceedings of the IEEE/CVF Conference on Computer Vision and Pattern Recognition (CVPR)*, 2021. 2, 5, 10, 11, 13, 14
- [80] Xintao Wang, Liangbin Xie, Chao Dong, and Ying Shan. Real-esrgan: Training real-world blind super-resolution with pure synthetic data. In *Proceedings of the IEEE/CVF International Conference on Computer Vision (ICCV)*, pages 1905–1914, 2021. 2
- [81] Xinlong Wang, Xiaosong Zhang, Zhengxiong Luo, Quan Sun, Yufeng Cui, Jinsheng Wang, Fan Zhang, Yueze Wang, Zhen Li, Qiying Yu, et al. Emu3: Next-token prediction is all you need. *arXiv preprint arXiv:2409.18869*, 2024. 3
- [82] Yufei Wang, Wenhan Yang, Xinyuan Chen, Yaohui Wang, Lanqing Guo, Lap-Pui Chau, Ziwei Liu, Yu Qiao, Alex C Kot, and Bihan Wen. Sinsr: diffusion-based image super-resolution in a single step. In *Proceedings of the IEEE/CVF Conference on Computer Vision and Pattern Recognition (CVPR)*, pages 25796–25805, 2024. 3, 5, 6, 7, 10, 11, 12, 13, 14
- [83] Zhou Wang, Alan C Bovik, Hamid R Sheikh, and Eero P Simoncelli. Image quality assessment: from error visibility to structural similarity. *IEEE Transactions on Image Processing (TIP)*, 13(4):600–612, 2004. 2, 7, 10
- [84] Chen Wei, Wenjing Wang, Wenhan Yang, and Jiaying Liu. Deep retinex decomposition for low-light enhancement. In *Proceedings of the British Machine Vision Conference (BMVC)*, 2018. 2, 3
- [85] Hongyang Wei, Shuaizheng Liu, Chun Yuan, and Lei Zhang. Perceive, understand and restore: Real-world image super-resolution with autoregressive multimodal generative models. In *Proceedings of the IEEE/CVF International Conference on Computer Vision (ICCV)*, 2025. 4, 5, 6, 7, 10, 11, 12, 13, 14
- [86] Pengxu Wei, Ziwei Xie, Hannan Lu, Zongyuan Zhan, Qixiang Ye, Wangmeng Zuo, and Liang Lin. Component divide-and-conquer for real-world image super-resolution. In *Proceedings of the European Conference on Computer Vision (ECCV)*, pages 101–117. Springer, 2020. 7, 9
- [87] Chengyue Wu, Xiaokang Chen, Zhiyu Wu, Yiyang Ma, Xingchao Liu, Zizheng Pan, Wen Liu, Zhenda Xie, Xingkai Yu, Chong Ruan, et al. Janus: Decoupling visual encoding for unified multimodal understanding and generation. *arXiv preprint arXiv:2410.13848*, 2024. 2, 3
- [88] Haoning Wu, Zicheng Zhang, Erli Zhang, Chaofeng Chen, Liang Liao, Annan Wang, Kaixin Xu, Chunyi Li, Jingwen Hou, Guangtao Zhai, et al. Q-instruct: Improving low-level visual abilities for multi-modality foundation models. In *Proceedings of the IEEE/CVF Conference on Computer Vision and Pattern Recognition (CVPR)*, pages 25490–25500, 2024. 3
- [89] Haoning Wu, Zicheng Zhang, Weixia Zhang, Chaofeng Chen, Liang Liao, Chunyi Li, Yixuan Gao, Annan Wang, Erli Zhang, Wenxiu Sun, et al. Q-align: Teaching LMMs for visual scoring via discrete text-defined levels. In *Proceedings of the International Conference on Machine Learning (ICML)*, 2024. 2, 3, 8
- [90] Haoning Wu, Hanwei Zhu, Zicheng Zhang, Erli Zhang, Chaofeng Chen, Liang Liao, Chunyi Li, Annan Wang, Wenxiu Sun, Qiong Yan, et al. Towards open-ended visual quality comparison. In *Proceedings of the European Conference on Computer Vision (ECCV)*, pages 360–377. Springer, 2024. 3
- [91] Haoning Wu, Zicheng Zhang, Erli Zhang, Chaofeng Chen, Liang Liao, Annan Wang, Chunyi Li, Wenxiu Sun, Qiong Yan, Guangtao Zhai, et al. Q-bench: A benchmark for general-purpose foundation models on low-level vision. In *Proceedings of the International Conference on Learning Representations (ICLR)*, 2025. 3
- [92] Rongyuan Wu, Lingchen Sun, Zhiyuan Ma, and Lei Zhang. One-step effective diffusion network for real-world image super-resolution. In *Proceedings of the Advances in Neural Information Processing Systems (NeurIPS)*, 2024. 5, 6, 7, 10, 11, 12, 13, 14
- [93] Rongyuan Wu, Tao Yang, Lingchen Sun, Zhengqiang Zhang, Shuai Li, and Lei Zhang. Seesr: Towards semantics-aware real-world image super-resolution. In *Proceedings of the IEEE/CVF Conference on Computer Vision and Pattern Recognition (CVPR)*, pages 25456–25467, 2024. 3, 5, 6, 7, 10, 11, 12, 13, 14
- [94] Tianhe Wu, Jian Zou, Jie Liang, Lei Zhang, and Kede Ma. Visualquality-r1: Reasoning-induced image quality assessment via reinforcement learning to rank. In *Proceedings of the Advances in Neural Information Processing Systems (NeurIPS)*, 2025. 3
- [95] Bin Xia, Yulun Zhang, Shiyin Wang, Yitong Wang, Xinglong Wu, Yapeng Tian, Wenming Yang, and Luc Van Gool. Diffir: Efficient diffusion model for image restoration. In *Proceedings of the IEEE/CVF Conference on Computer Vision and Pattern Recognition (CVPR)*, 2023. 2, 3, 7, 8, 12, 14, 15
- [96] Jinheng Xie, Weijia Mao, Zechen Bai, David Junhao Zhang, Weihao Wang, Kevin Qinghong Lin, Yuchao Gu, Zhijie Chen, Zhenheng Yang, and Mike Zheng Shou. Show-o: One single transformer to unify multimodal understanding and generation. In *Proceedings of the International Conference on Learning Representations (ICLR)*, 2025. 2, 3
- [97] Sidi Yang, Tianhe Wu, Shuwei Shi, Shanshan Lao, Yuan Gong, Mingdeng Cao, Jiahao Wang, and Yujiu Yang. Maniqa: Multi-dimension attention network for no-reference image quality assessment. In *Proceedings of the IEEE/CVF Conference on Computer Vision and Pattern Recognition (CVPR)*, pages 1191–1200, 2022. 2, 7, 8, 10
- [98] Tao Yang, Rongyuan Wu, Peiran Ren, Xuansong Xie, and Lei Zhang. Pixel-aware stable diffusion for realistic image super-resolution and personalized stylization. In *European conference on computer vision*, pages 74–91, 2024. 5, 6, 7, 10, 11, 13, 14
- [99] Zhiyuan You, Jinjin Gu, Zheyuan Li, Xin Cai, Kaiwen Zhu, Chao Dong, and Tianfan Xue. Descriptive image quality

- assessment in the wild. *arXiv preprint arXiv:2405.18842*, 2024. 2, 3, 4
- [100] Zhiyuan You, Zheyuan Li, Jinjin Gu, Zhenfei Yin, Tianfan Xue, and Chao Dong. Depicting beyond scores: Advancing image quality assessment through multi-modal language models. In *Proceedings of the European Conference on Computer Vision (ECCV)*, pages 259–276. Springer, 2024. 2, 3
- [101] Zhiyuan You, Xin Cai, Jinjin Gu, Tianfan Xue, and Chao Dong. Teaching large language models to regress accurate image quality scores using score distribution. In *Proceedings of the IEEE/CVF Conference on Computer Vision and Pattern Recognition (CVPR)*, 2025. 2, 3, 8
- [102] Fanghua Yu, Jinjin Gu, Zheyuan Li, Jinfan Hu, Xiangtao Kong, Xintao Wang, Jingwen He, Yu Qiao, and Chao Dong. Scaling up to excellence: Practicing model scaling for photo-realistic image restoration in the wild. In *Proceedings of the IEEE/CVF Conference on Computer Vision and Pattern Recognition (CVPR)*, 2024. 3, 7, 8, 12, 14, 15
- [103] Zongsheng Yue, Jianyi Wang, and Chen Change Loy. Resshift: Efficient diffusion model for image super-resolution by residual shifting. *Proceedings of the Advances in Neural Information Processing Systems (NeurIPS)*, 36, 2024. 3, 5, 6, 7, 10, 11, 13, 14
- [104] Zongsheng Yue, Kang Liao, and Chen Change Loy. Arbitrary-steps image super-resolution via diffusion inversion. In *Proceedings of the IEEE/CVF Conference on Computer Vision and Pattern Recognition (CVPR)*, pages 23153–23163, 2025. 10, 11
- [105] Syed Waqas Zamir, Aditya Arora, Salman Khan, Munawar Hayat, Fahad Shahbaz Khan, and Ming-Hsuan Yang. Restormer: Efficient transformer for high-resolution image restoration. In *Proceedings of the IEEE/CVF Conference on Computer Vision and Pattern Recognition (CVPR)*, 2022. 7, 8, 12, 14, 15
- [106] Aiping Zhang, Zongsheng Yue, Renjing Pei, Wenqi Ren, and Xiaochun Cao. Degradation-guided one-step image super-resolution with diffusion priors. *arXiv preprint arXiv:2409.17058*, 2024. 5, 6, 7, 10, 11, 12, 13, 14
- [107] Jinghao Zhang, Jie Huang, Mingde Yao, Zizheng Yang, Hu Yu, Man Zhou, and Feng Zhao. Ingredient-oriented multi-degradation learning for image restoration. In *Proceedings of the IEEE/CVF Conference on Computer Vision and Pattern Recognition (CVPR)*, 2023. 14, 15
- [108] Kai Zhang, Jingyun Liang, Luc Van Gool, and Radu Timofte. Designing a practical degradation model for deep blind image super-resolution. In *Proceedings of the IEEE/CVF International Conference on Computer Vision (ICCV)*, pages 4791–4800, 2021. 12
- [109] Lin Zhang, Lei Zhang, Xuanqin Mou, and David Zhang. Fsim: A feature similarity index for image quality assessment. *IEEE Transactions on Image Processing (TIP)*, 20(8):2378–2386, 2011. 2
- [110] Lin Zhang, Lei Zhang, and Alan C Bovik. A feature-enriched completely blind image quality evaluator. *IEEE Transactions on Image Processing (TIP)*, 24(8):2579–2591, 2015. 2, 7, 10
- [111] Richard Zhang, Phillip Isola, Alexei A Efros, Eli Shechtman, and Oliver Wang. The unreasonable effectiveness of deep features as a perceptual metric. In *Proceedings of the IEEE/CVF Conference on Computer Vision and Pattern Recognition (CVPR)*, pages 586–595, 2018. 2
- [112] Weixia Zhang, Guangtao Zhai, Ying Wei, Xiaokang Yang, and Kede Ma. Blind image quality assessment via vision-language correspondence: A multitask learning perspective. In *Proceedings of the IEEE/CVF Conference on Computer Vision and Pattern Recognition (CVPR)*, pages 14071–14081, 2023. 7, 10
- [113] Xuanyu Zhang, Weiqi Li, Shijie Zhao, Junlin Li, Li Zhang, and Jian Zhang. Vq-insight: Teaching vlms for ai-generated video quality understanding via progressive visual reinforcement learning. In *Proceedings of the AAAI Conference on Artificial Intelligence (AAAI)*, 2025. 2, 3
- [114] Yulun Zhang, Kunkeng Li, Kai Li, Lichen Wang, Bineng Zhong, and Yun Fu. Image super-resolution using very deep residual channel attention networks. In *Proceedings of the European Conference on Computer Vision (ECCV)*, pages 286–301, 2018. 2
- [115] Zicheng Zhang, Ziheng Jia, Haoning Wu, Chunyi Li, Zijian Chen, Yingjie Zhou, Wei Sun, Xiaohong Liu, Xiongkuo Min, Weisi Lin, et al. Q-bench-video: Benchmarking the video quality understanding of llms. In *Proceedings of the IEEE/CVF Conference on Computer Vision and Pattern Recognition (CVPR)*, 2025. 3
- [116] Zicheng Zhang, Tengchuan Kou, Shushi Wang, Chunyi Li, Wei Sun, Wei Wang, Xiaoyu Li, Zongyu Wang, Xuezhi Cao, Xiongkuo Min, et al. Q-eval-100k: Evaluating visual quality and alignment level for text-to-vision content. *arXiv preprint arXiv:2503.02357*, 2025.
- [117] Zicheng Zhang, Haoning Wu, Ziheng Jia, Weisi Lin, and Guangtao Zhai. Teaching llms for image quality scoring and interpreting. *arXiv preprint arXiv:2503.09197*, 2025. 3
- [118] Shijie Zhao, Xuanyu Zhang, Weiqi Li, Junlin Li, Li Zhang, Tianfan Xue, and Jian Zhang. Reasoning as representation: Rethinking visual reinforcement learning in image quality assessment. *arXiv preprint arXiv:2510.11369*, 2025. 3
- [119] Dian Zheng, Xiao-Ming Wu, Shuzhou Yang, Jian Zhang, Jian-Fang Hu, and Wei-Shi Zheng. Selective hourglass mapping for universal image restoration based on diffusion model. In *Proceedings of the IEEE/CVF Conference on Computer Vision and Pattern Recognition (CVPR)*, 2024. 2, 3, 7, 8, 12, 14, 15
- [120] Heliang Zheng, Huan Yang, Jianlong Fu, Zheng-Jun Zha, and Jiebo Luo. Learning conditional knowledge distillation for degraded-reference image quality assessment. In *Proceedings of the IEEE/CVF International Conference on Computer Vision (ICCV)*, pages 10242–10251, 2021. 3
- [121] Chunting Zhou, Lili Yu, Arun Babu, Kushal Tirumala, Michihiro Yasunaga, Leonid Shamir, Jacob Kahn, Xuezhe Ma, Luke Zettlemoyer, and Omer Levy. Transfusion: Predict the next token and diffuse images with one multi-modal model. *arXiv preprint arXiv:2408.11039*, 2024. 2, 3
- [122] Shangchen Zhou, Chongyi Li, and Chen Change Loy. Led-net: Joint low-light enhancement and deblurring in the dark.

In *Proceedings of the European Conference on Computer Vision (ECCV)*, 2022. [2](#), [3](#)

- [123] Hancheng Zhu, Leida Li, Jinjian Wu, Weisheng Dong, and Guangming Shi. Metaiqa: Deep meta-learning for no-reference image quality assessment. In *Proceedings of the IEEE/CVF Conference on Computer Vision and Pattern Recognition (CVPR)*, pages 14143–14152, 2020. [3](#)